physics

MDPI

Review

Higgs Boson Searches at the LHC Beyond the Standard Model

André Sopczak

Institute of Experimental and Applied Physics, Czech Technical University in Prague, Husova 240/5, 11000 Prague, Czech Republic; andre.sopczak@cern.ch

Abstract: The latest results of Higgs boson searches beyond the Standard Model from the ATLAS and CMS experiments are reviewed. This includes searches for additional neutral, charged, and double charged Higgs-like bosons, searches for dark matter produced in association with a Higgs boson, and searches for new physics in Higgs boson production and decay processes. Interpretations are given within the hMSSM, a special parameterization of the Minimal Supersymmetric extension of the Standard Model, in which the mass of the lightest Higgs boson is set to the value of 125 GeV measured at the LHC.

Keywords: beyond Standard Model searches; Higgs bosons; LHC; ATLAS; CMS

Citation: Sopczak, A. Higgs Boson Searches at the LHC Beyond the Standard Model . *Physics* **2024**, *6*, 1132–1170. https://doi.org/10.3390/physics6030071

Received: 10 March 2024
Revised: 25 May 2024
Accepted: 4 June 2024
Published: 19 September 2024

1. Introduction

Since the discovery of the Higgs boson with the properties of the Standard Model in 2012 [1,2], a number searches for Higgs bosons beyond the Standard Model have been made. These searches can be organized according to different proposed extensions of the Higgs sector [3]. Two-Higgs-Doublet Models (2HDMs) introduce five Higgs bosons: two scalar (h, H), a pseudoscalar (A) neutral, and two ($H^{\pm}$) charged particles. The Minimal Supersymmetric extension of the SM (MSSM) is a 2HDM that can contain additional particles within reach of the Large Hadron Collider (LHC), namely the superpartners of SM particles. The 2HDMs with an extra light singlet (a) bring new phenomena through the opening of the decay $H \to aa$. Three-HDMs (3HDMs) enlarge the Higgs boson sector, having three charge-parity CP-even and two CP-odd neutral Higgs bosons, as well as two charged Higgs bosons. In models with an additional $U(1)_D$ gauge symmetry, a pseudoscalar (A) and charged Higgs bosons ($H^{\pm}$) are predicted. In Type-II seesaw models, left–right symmetric models (LRSMs), the Zee–Babu neutrino mass model, 3-3-1 models, and the Georgi–Machacek model, doubly charged Higgs (H^{++}) are predicted.

A previous review of the SM Higgs boson research was given at the 2019 International Conference on Precision Physics and Fundamental Physical Constants, FFK2019 [4].

This review is structured as follows. Section 2 describes Higgs boson decays. Section 3 is devoted to the enhanced production modes. Section 4 describes Higgs boson resonance production searches. Section 5 reports on the additional neutral Higgs boson production. Section 6 reports on the Higgs boson dark matter production. Section 7 reports on the charged Higgs boson production searches. Interpretations and outlook are given in Section 8.

1.1. LHC, Experiments, and Data Taking

The data from proton–proton collisions at the LHC at CERN have been recorded with the ATLAS and CMS experiments in three data taking periods:

- LHC Run-1: 2010–2012, discovery of the Higgs boson [1,2];
- LHC Run-2: 2015–2018, results presented here;
- LHC Run-3: 2022–2025, ongoing data taking.

Figure 1 illustrates the layout of the LHC (Figure 1, left) and of the ATLAS and CMS experiments (Figure 1, right). The LHC location of the underground area is shown, as well as the terrain.

Figure 2, left, shows the luminosity delivered to the ATLAS experiment from proton–proton collisions, while Figure 2, right, shows a schematic view of particle identification in the ATLAS or CMS detectors.

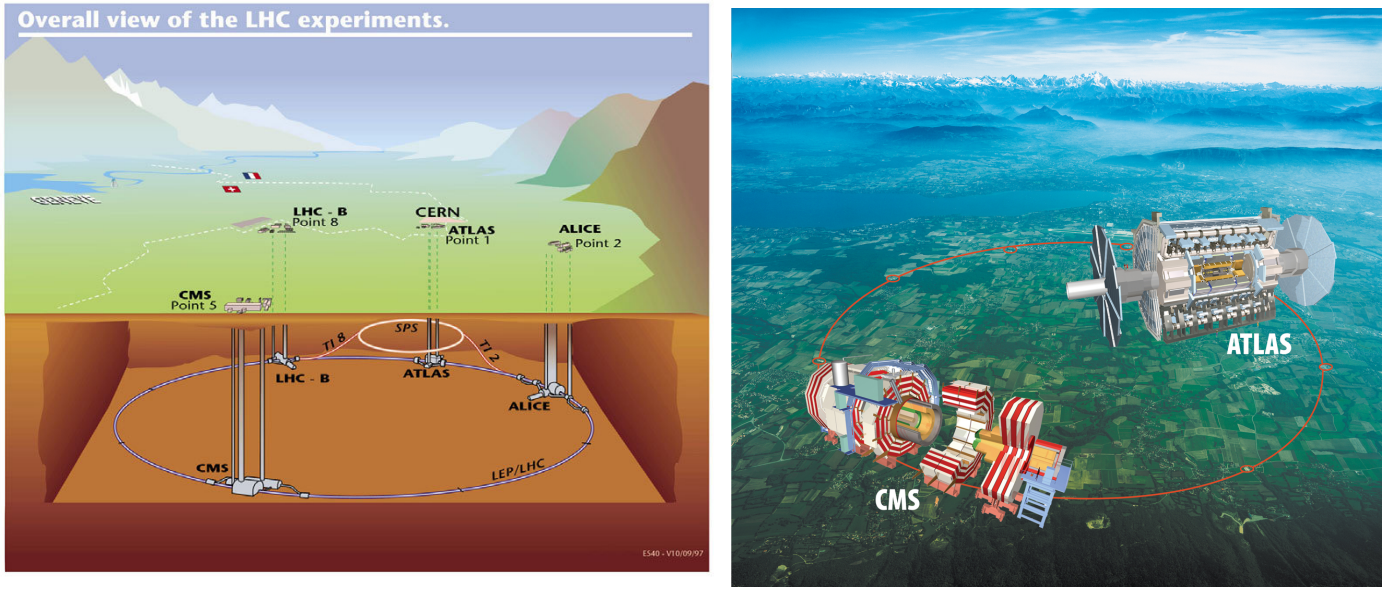

Figure 1. Left: LHC underground and terrain areas with four experiments. **Right**: ATLAS and CMS experiments.

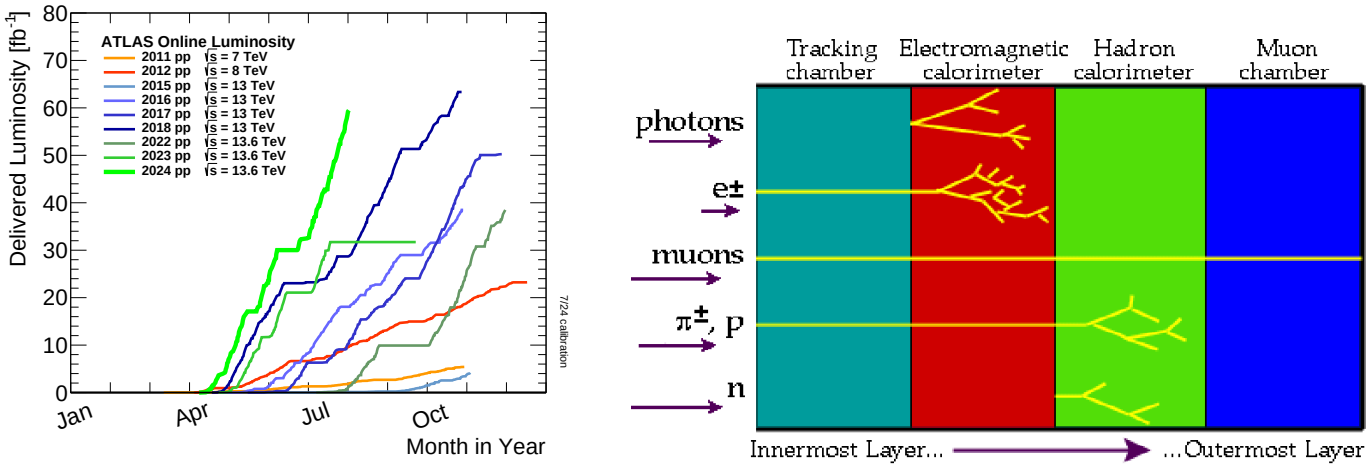

Figure 2. Left: delivered luminosity at the ATLAS experiment [5]. Reproduced under the CC-BY-4.0 license. **Right**: particle identification schema by different subsystems.

Event displays of typical recorded proton–proton collisions are shown in Figure 3. The proton–proton collisions in the center of the detectors lead to different reactions, including the production of the SM Higgs boson and potentially the production of the Higgs boson predicted in extended models.

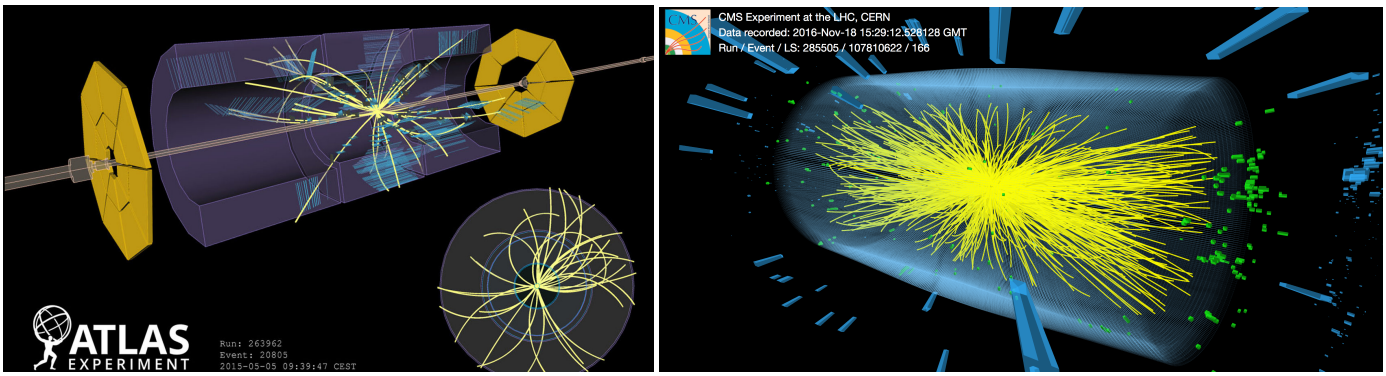

Figure 3. Event displays from the (**left**) ATLAS [6]. and (**right**) CMS [7] experiments. Reproduced under the CC-BY-4.0 license.

1.2. Production Modes

The analyses presented here are mostly based on the full LHC Run-2 dataset. The evolution of the integrated luminosity recorded by the CMS experiment as a function of time is shown in Figure 4 along with the number of expected SM Higgs boson events in the production modes ggH, VBF, VH, ttH, tH, and HH in Table 1 where g denotes gluon, VBF denotes vector boson fusion, and t denotes the top quark. The corresponding Feynman diagrams are shown in Figures 5–7 along with the production cross-sections for 13 TeV center-of-mass energy [8] and the resulting expected rates for 140 fb^{-1} integrated luminosity [9]. The expected rates can vary in different extensions of the SM.

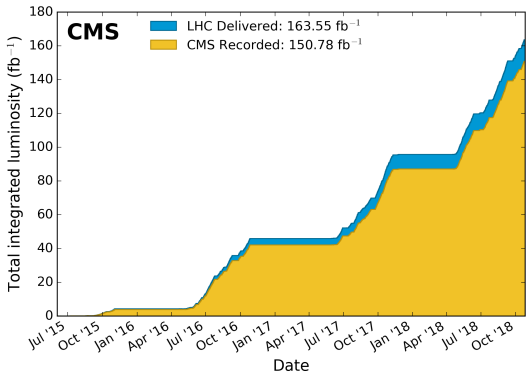

Figure 4. LHC Run-2 integrated luminosity [10]. Reproduced under the CC-BY-4.0 license.

Table 1. Expected numbers of Higgs boson events. See text for details.

Mode	Events ×1000	Fraction (%)
ggH	6900	88.19
VBF	520	6.65
VH	320	4.09
ttH	70	0.89
tH	10	0.13
HH	4	0.05
sum	7824	

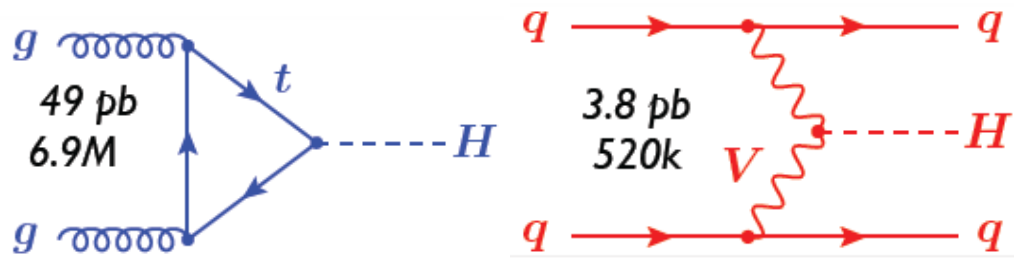

Figure 5. Feynman diagrams for ggH (**left**) and VBF (**right**) Higgs boson production modes (see text for details). The production cross-sections (in pb) are given for 13 TeV center-of-mass energy [8] and the expected rates ("M" stands for "$\times 10^6$" and "k" stands for "$\times 10^3$") are given for 140 fb^{-1} integrated luminosity [9].

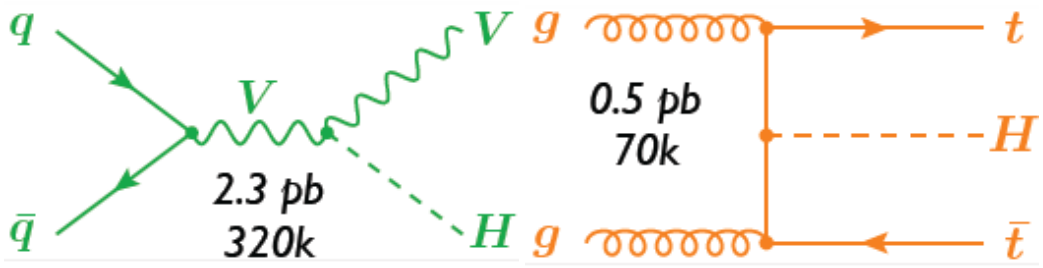

Figure 6. Feynman diagrams for VH (**left**) and ttH (**right**) Higgs boson production modes (see text for details). The production cross-sections (in pb) are given for 13 TeV center-of-mass energy [8] and the expected rates ("k" stands for $\times 10^3$) are given for 140 fb^{-1} integrated luminosity [9].

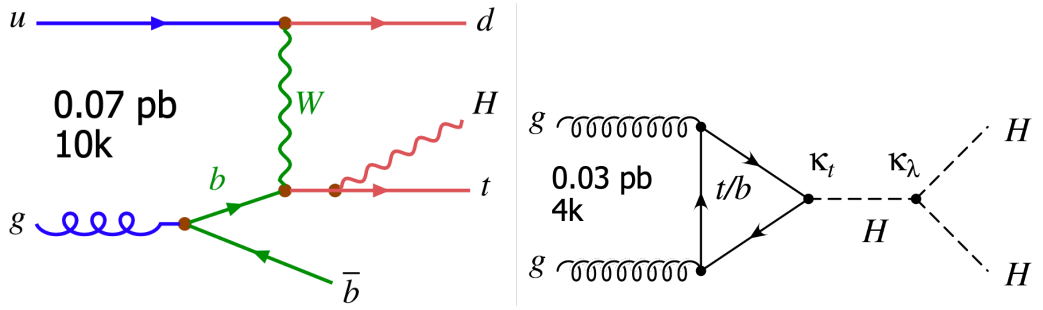

Figure 7. Feynman diagrams for tH (**left**) and HH (**right**) Higgs boson production modes (see text for details). The production cross-sections (in pb) are given for 13 TeV center-of-mass energy [8] and the expected rates ("k" stands for $\times 10^3$) are given for 140 fb^{-1} integrated luminosity [9].

1.3. Decay Branching Ratios

SM predictions for the Higgs boson branching ratios and precision measurements for several Higgs boson decay modes are summarized in Table 2 [8] and Figure 8 [11], respectively. Physics beyond the SM (BSM) may change these ratios. After establishing the main decay channels and striving to precisely characterize them, the experimental focus is now on the measurements of the rare decay modes that can be enhanced in extended models.

1.4. Relation of Coupling to Fermion/Vector Boson Mass

The relationships between couplings and fermions and vector bosons as a function of the particle masses measured by ATLAS and CMS experiments [11,12] are shown in Figure 9. The SM expectation and the measurements are in remarkable agreement within the uncertainties (the smallest of which is about 3% for WW/ZZ boson couplings).

Table 2. Theoretical predictions of Higgs boson decay branching ratios in the SM [8]. Reproduced under the CC-BY-4.0 license.

Decay Channel	BR (%)
bb	57.63 ± 0.70
WW	22.00 ± 0.33
gg	8.15 ± 0.42
$\tau\tau$	6.21 ± 0.09
cc	2.86 ± 0.09
ZZ	2.71 ± 0.04
$\gamma\gamma$	0.227 ± 0.005
$Z\gamma$	0.157 ± 0.009
ss	0.025 ± 0.001
$\mu\mu$	0.0216 ± 0.0004

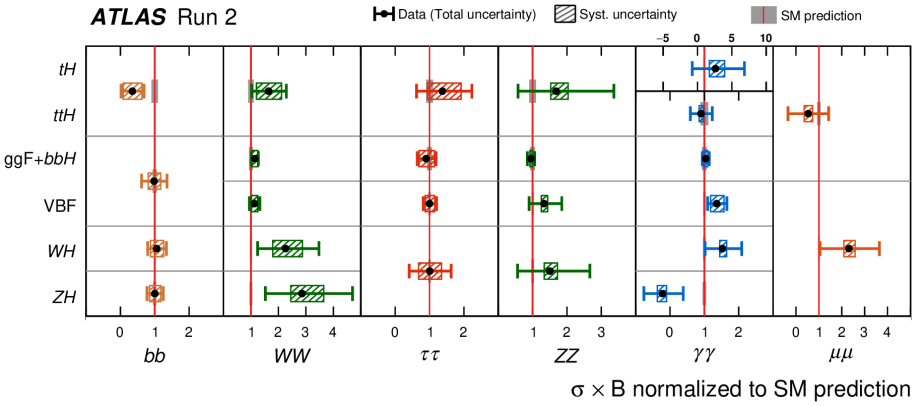

Figure 8. Cross-section times branching ratio measurements [11]. Reproduced under the copyright permission from Springer Nature.

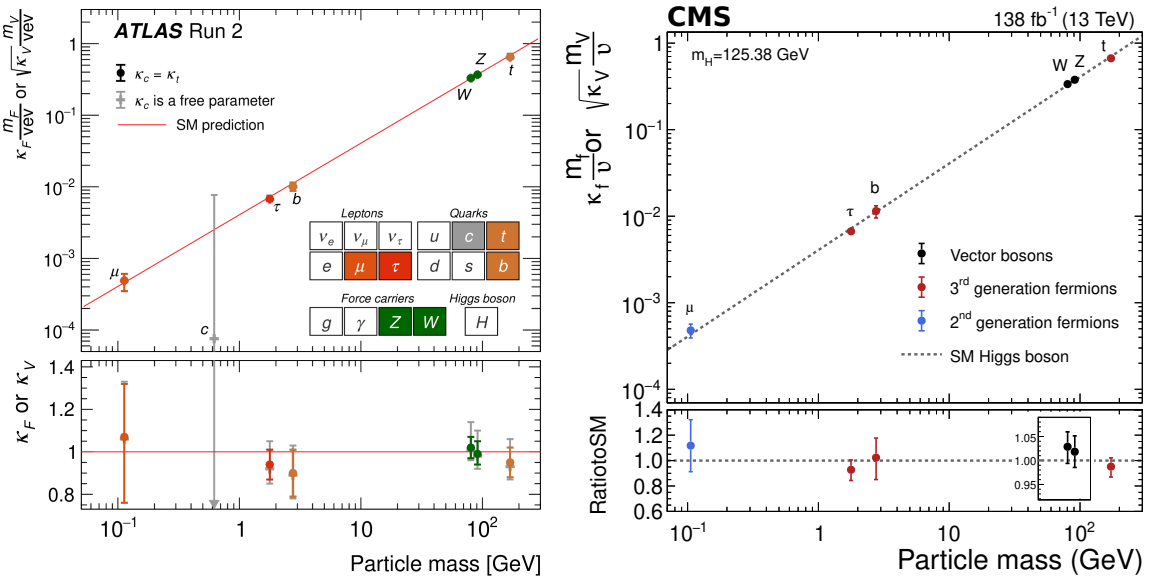

Figure 9. Relationships between couplings and fermion/vector boson masses by (**left**) ATLAS [11] and (**right**) CMS [12] experiments. Reproduced under the copyright permission from Springer Nature.

1.5. Higgs Boson Width

The width of the Higgs boson can be measured using the ZZ production mode and subsequent decay, including virtual Higgs boson contributions and its interference [13]. The two sensitive processes are $ZZ \to 4\ell$ and $ZZ \to 2\ell 2\nu$, with $\ell = e$ or μ. Figure 10

shows Feynman diagrams of ZZ ($V = Z$) production and the simulated ZZ differential cross-section as a function of the four-lepton invariant mass [13]. The contribution of the Higgs boson allows determing the Higgs boson width. The ATLAS experiment indirect limit on the width measurement is $\Gamma = 3.4^{+3.3}_{-2.5}$ MeV, with an observed upper limit of 10.5 MeV, for an expected value of 10.9 MeV at 95% CL [14] and $\Gamma = 3.2^{+2.4}_{-1.7}$ MeV for the CMS [13] experiment. Both measurements are in good agreement with the SM prediction $\Gamma = 4.1$ MeV [8]. The corresponding likelihood is shown in Figure 11 [13,14], assuming no new particles enter in the production of the virtual Higgs boson.

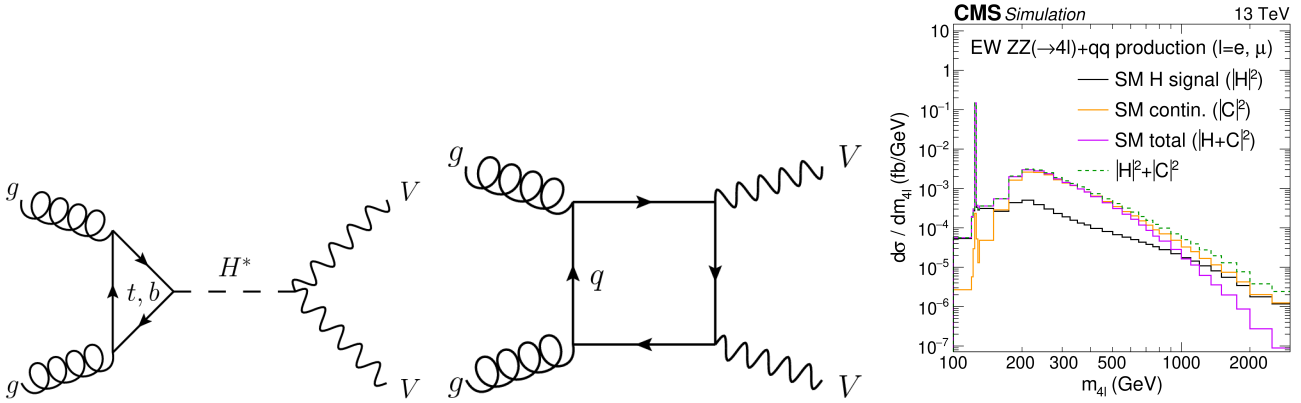

Figure 10. Left and **Middle**: Feynman diagrams of VV production. **Right**: simulated differential ZZ production cross-section as a function of the four-lepton invariant mass [13]. Reproduced under the copyright permission from Springer Nature.

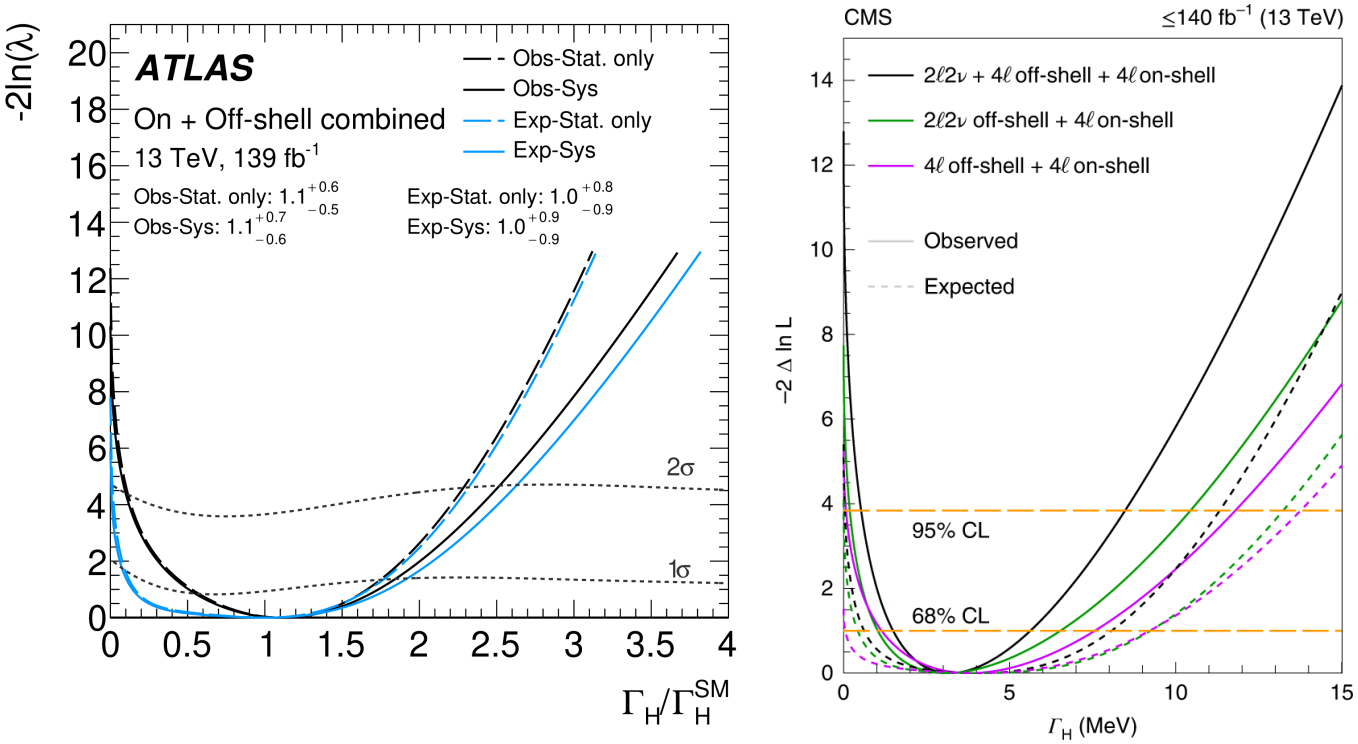

Figure 11. Likelihood for Higgs boson width measurements by (**left**) ATLAS [14] and (**right**) CMS [13] experiments. Reproduced under the copyright permission from Elsevier (**left**) and Springer Nature (**right**).

1.6. Higgs Boson CP Properties

A study of the CP properties of the interaction between the Higgs boson and tau-leptons (τs) was performed, based on the reconstruction of the planes of tau decay products. The results of the observed signal strength $\mu_{\tau\tau}$ versus the CP-mixing angle ϕ_τ are shown in Figure 12, right [15]. No indication of a non-SM contribution is observed. To clarify, Figure 12, left, presents the definition of the φ^*_{CP} angle and Figure 12, middle, shows the data and simulation distribution. The Lagrangian defining ϕ_τ and κ_τ reads $\mathcal{L}_{H\tau\tau} = \frac{m_\tau}{v}\kappa_\tau(\cos\phi_\tau\bar{\tau}\tau + \sin\phi_\tau\,\bar{\tau}\,i\,\gamma_5\tau)H$ [15], and $\mu_{\tau\tau}$ is the ratio of the signal strength to the SM expectation.

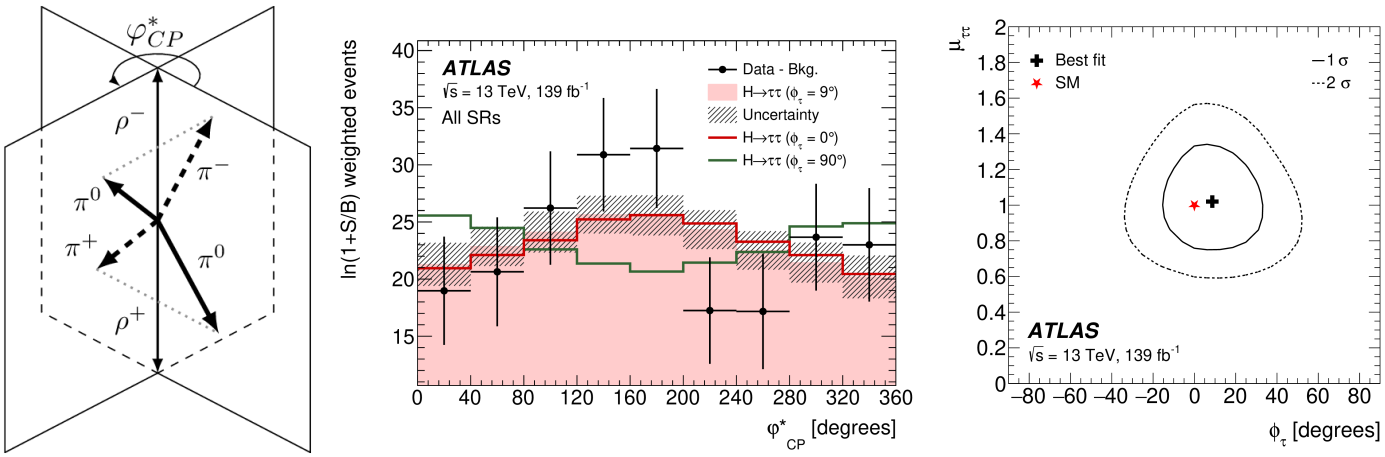

Figure 12. Left: definition of the angle between τ-decay products. **Middle**: measured and simulated angle distributions between τ-decay products [15]. **Right**: observed and expected signal strength, $\mu_{\tau\tau}$, versus the CP-mixing angle ϕ_τ [15]. Reproduced under the copyright permission from Springer.

The CP structure of the Higgs boson top quark Yukawa coupling was also measured in tH and ttH production [16]. The parameters $\kappa_t = 0$ (CP-even) and $\kappa_t = 1$ (CP-odd) are used, and other parameters are fixed to their SM values. Figure 13, left, compares the distributions of the ttH invariant mass for the pure CP-even and CP-odd assumptions and Figure 13, middle, and Table 3 show the results of the measured κ_t and $\tilde{\kappa}_t$ values [16].

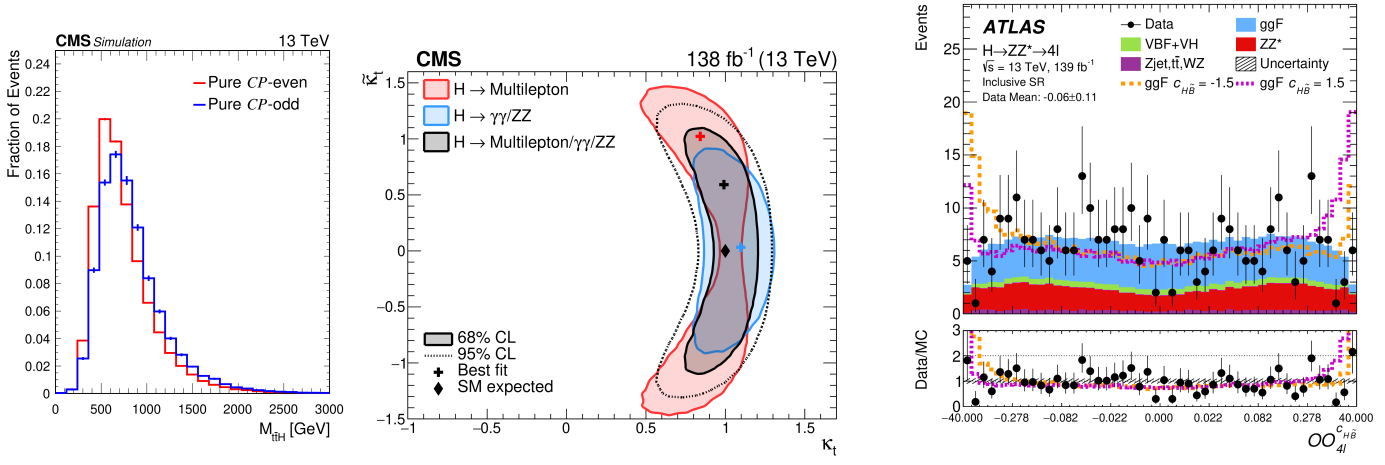

Figure 13. Left: comparison of the distributions of the ttH invariant mass for the pure CP-even and CP-odd assumptions [16]. **Middle**: observed and SM expected κ_t and $\tilde{\kappa}_t$ values [16]. **Right**: decay level observable for CP-invariance in ggF VBF production for $H \to ZZ \to 4\ell$ [17]. See text for details. Reproduced under the copyright permission from Springer.

Table 3. Limits on measured κ_t and $\tilde{\kappa}_t$ values [16]. See text for details. Reproduced under the copyright permission from Springer.

Parameter	68% CL	95% CL
κ_t	(0.96, 1.16)	(0.86, 1.26)
$\tilde{\kappa}_t$	(−0.86, 0.85)	(−1.07, 1.07)

The CP properties in ggF and VBF production for $H \to ZZ \to 4\ell$ have been studied in Ref. [17]. Matrix element-based optimal observables were used to constrain CP-odd couplings beyond the SM in the framework of SM effective field theory [18]. The tested CP-invariance of Higgs boson interactions with VH ($V = W, Z$) were performed. Results are compatible with the SM expectation, and no hint of BSM physics was observed. Figure 13, right, compares data and simulation for $H \to ZZ \to 4\ell$ [17].

2. Higgs Boson Decay

Higgs boson couplings beyond the already observed tt, ZZ, WW, bb, $\tau\tau$, and $\mu\mu$ couplings are discussed here.

2.1. $H \to ee$

Higgs boson decays into a pair of electrons having a quite small branching fraction in the SM BR$(H \to ee) \approx 5 \times 10^{-9}$. The branching fraction could be enhanced in the 2HDM, and experimental limits are set to BR $(H \to ee) < 3.0 \times 10^{-4}$ (3.0×10^{-4} expectation) at 95% CL [19] when the various measurements are combined, as shown in Figure 14, left. The reconstructed di-electron mass distribution does not yet show a visible signal due to the expected low rate; see Figure 14, right.

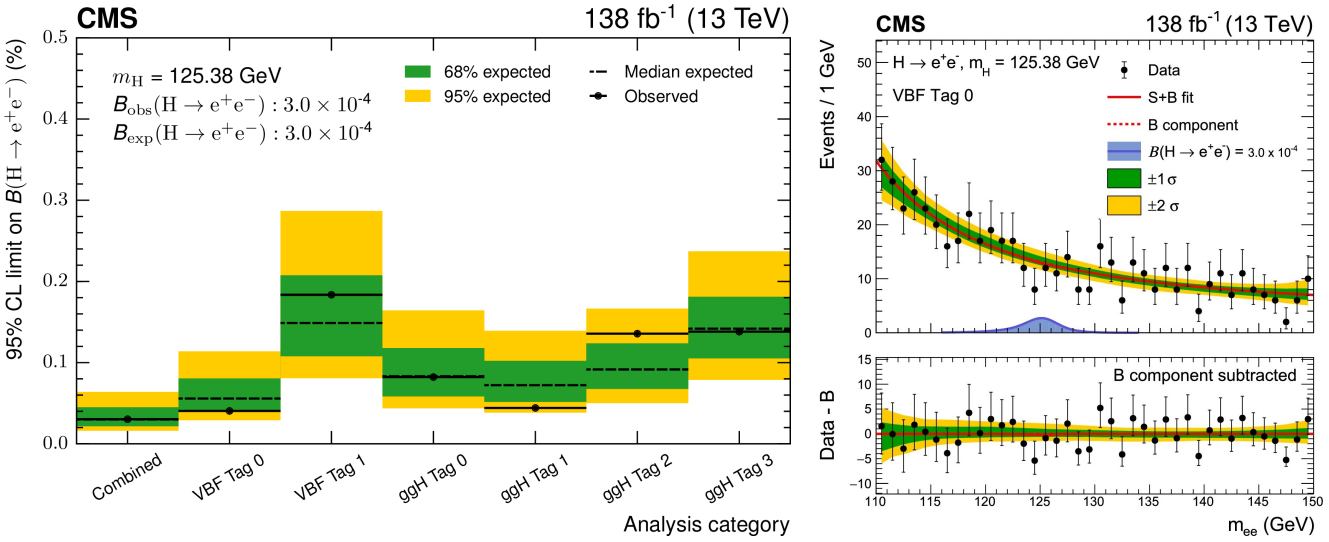

Figure 14. Left: upper limits on the $H \to ee$ branching ratio in various search channels and those combined [19]. **Right**: reconstructed di-electron mass distributon [19]. Reproduced under the copyright permission from Elsevier.

2.2. $H \to Z\gamma$

The $H \to Z\gamma$ SM Higgs boson decay modes are within experimental reach. The ATLAS Collaboration obtains a significance of 2.2 (1.2 exp.) standard deviation (s.d.), and the best-fit value for the signal yield normalized to the SM prediction is $\mu = 2.0^{+1.0}_{-0.9}$ [20], while the CMS Collaboration obtains a significance of 2.7 (1.2 exp.) s.d. and $\mu = 2.4 \pm 0.9$ [21], where the statistical component of the uncertainty is dominant. Figure 15 shows the $Z\gamma$ distribution from ATLAS [20] (Figure 15, left) and CMS [21] (Figure 15, right) experiments, as well as an event display of an ATLAS experiment candidate event (Figure 15, middle). A

combination of the data from the ATLAS and CMS Collaborations leads to a 3.4 (1.6 exp.) s.d. evidence with $\mu = 2.2 \pm 0.7$ [22] (Figure 16, left).

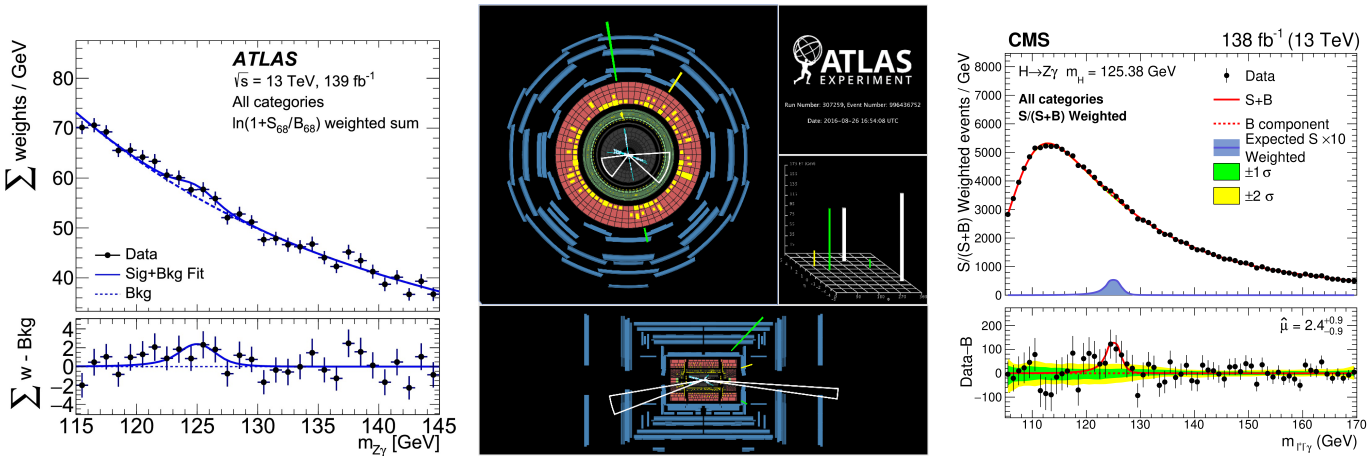

Figure 15. Left: ATLAS experiment $Z\gamma$ invariant-mass distribution [20]. **Middle**: ATLAS experiment $Z\gamma$ ($Z \to ee$) candidate event display [20]. **Right**: CMS experiment $Z\gamma$ invariant-mass distribution [21]. Reproduced under the copyright permission from Elsevier (left, middle) and Springer (right).

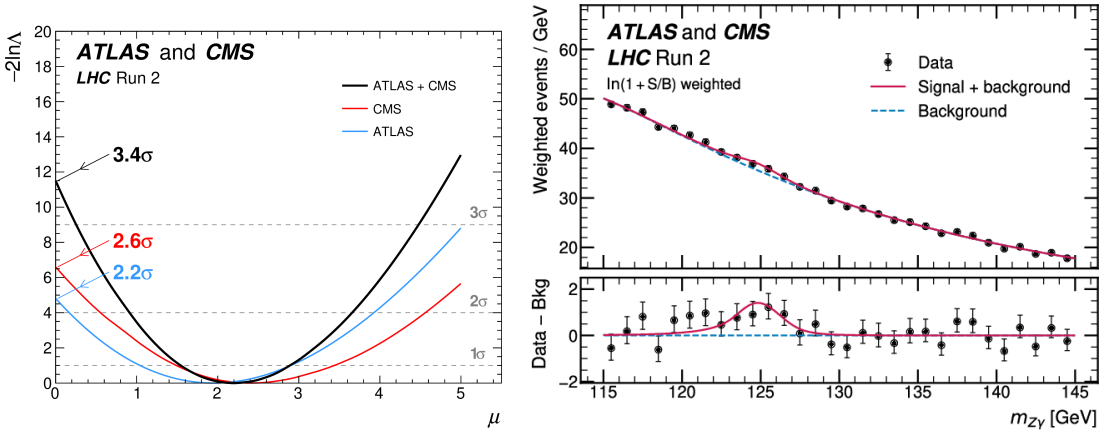

Figure 16. Left: negative profile log-likelihood test statistic as a function of the $Z\gamma$ signal strength μ [22], where σ denotes standard deviation. **Right**: ATLAS and CMS experiments $Z\gamma$ invariant mass distribution [22]. Reproduced under the copyright permission from the American Physical Society.

2.3. $H \to J/\psi J/\psi$, YY, ZJ/ψ

Further rare Higgs boson decays lead to four-muon final states. Experimentally, this has a clean signature owing to considerably small SM background. The expected sensitivity for the branching fractions is several orders of magnitude below the current experimental sensitivity. The observation of such decays indicates physics beyond the SM. Limits obtained are at 95% CL [23], as shown in Figure 17. Observed and expected limits are in quite a good agreement (Table 4).

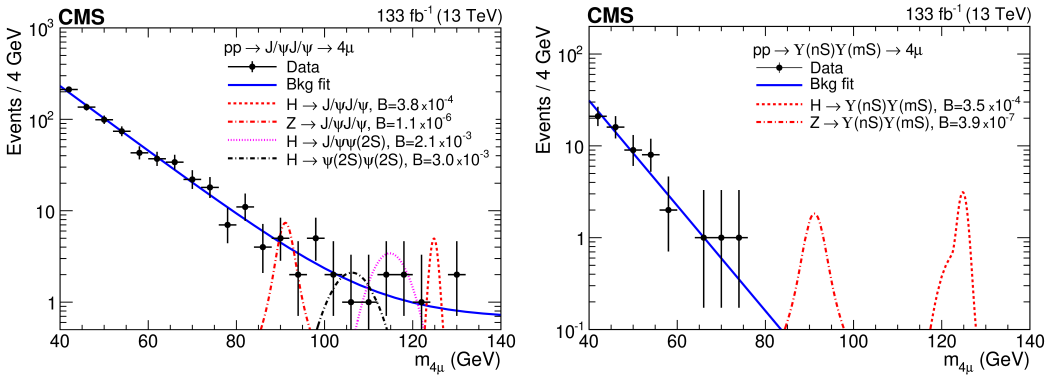

Figure 17. Left: four-muon invariant mass for $H \to J/\psi J/\psi$ searches. The limits are given for different assumptions on the polarization of the intermediate particles. The signal distributions are shown for branching ratios at the observed limit [23]. **Right**: four-muon invariant mass for $H \to YY$ searches [23]. Reproduced under the copyright permission from Elsevier.

Table 4. Observed and expected limits on Higgs boson branching ratios.

Process	**Observed**	**Expected**	**Observed**	
Higgs boson channel	Longitudinal	Longitudinal	Unpolarized	Transverse
$\mathcal{B}(\mathrm{H} \to \mathrm{ZJ}/\psi)$	1.9×10^{-3}	$(2.6^{+1.1}_{-0.7}) \times 10^{-3}$	2.4×10^{-3}	2.8×10^{-3}
$\mathcal{B}(\mathrm{H} \to \mathrm{Z}\psi(2\mathrm{S}))$	6.6×10^{-3}	$(7.1^{+2.8}_{-2.0}) \times 10^{-3}$	8.3×10^{-3}	9.4×10^{-3}
$\mathcal{B}(\mathrm{H} \to \mathrm{J}/\psi\mathrm{J}/\psi)$	3.8×10^{-4}	$(4.6^{+2.0}_{-0.6}) \times 10^{-4}$	4.7×10^{-4}	5.2×10^{-4}
$\mathcal{B}(\mathrm{H} \to \psi(2\mathrm{S})\mathrm{J}/\psi)$	2.1×10^{-3}	$(1.4^{+0.6}_{-0.4}) \times 10^{-3}$	2.6×10^{-3}	2.9×10^{-3}
$\mathcal{B}(\mathrm{H} \to \psi(2\mathrm{S})\psi(2\mathrm{S}))$	3.0×10^{-3}	$(3.3^{+1.5}_{-0.9}) \times 10^{-3}$	3.6×10^{-3}	4.7×10^{-3}
$\mathcal{B}(\mathrm{H} \to \Upsilon(\mathrm{nS})\Upsilon(\mathrm{mS}))$	3.5×10^{-4}	$(3.6^{+0.2}_{-0.3}) \times 10^{-4}$	4.3×10^{-4}	4.6×10^{-4}
$\mathcal{B}(\mathrm{H} \to \Upsilon(1\mathrm{S})\Upsilon(1\mathrm{S}))$	1.7×10^{-3}	$(1.7^{+0.1}_{-0.1}) \times 10^{-3}$	2.0×10^{-3}	2.2×10^{-3}
Z boson channel				
$\mathcal{B}(\mathrm{Z} \to \mathrm{J}/\psi\mathrm{J}/\psi)$	11×10^{-7}	$(9.5^{+3.8}_{-2.6}) \times 10^{-7}$	14×10^{-7}	16×10^{-7}
$\mathcal{B}(\mathrm{Z} \to \Upsilon(\mathrm{nS})\Upsilon(\mathrm{mS}))$	3.9×10^{-7}	$(4.0^{+0.3}_{-0.3}) \times 10^{-7}$	4.9×10^{-7}	5.6×10^{-7}
$\mathcal{B}(\mathrm{Z} \to \Upsilon(1\mathrm{S})\Upsilon(1\mathrm{S}))$	1.8×10^{-6}	$(1.8^{+0.1}_{-0.0}) \times 10^{-6}$	2.2×10^{-6}	2.4×10^{-6}

2.4. $H \to \omega\gamma$, $K^*\gamma$

Searches for Higgs boson decay to $\omega\gamma$, $K^*\gamma$ probe flavor-conserving and flavor-violating Higgs boson couplings to light quarks [24,25]. Figure 18, upper left, middle and right shows relevant Feynman diagrams and Figure 18, lower left and middle, shows invariant mass distributions, observed and expected limits. No excess of branching ratio is observed (see Table 5).

Table 5. Observed and expected limits: $H \to \omega\gamma$, $K^*\gamma$ [24].

Channel	**95% CL Upper Limit**	
	Expected	**Observed**
$H \to \omega\gamma[10^{-4}]$	$3.0^{+1.2}_{-0.8}$	1.5
$Z \to \omega\gamma[10^{-7}]$	$5.7^{+2.3}_{-1.6}$	3.8
$H \to K^*\gamma[10^{-5}]$	$12.2^{+4.9}_{-3.4}$	8.9

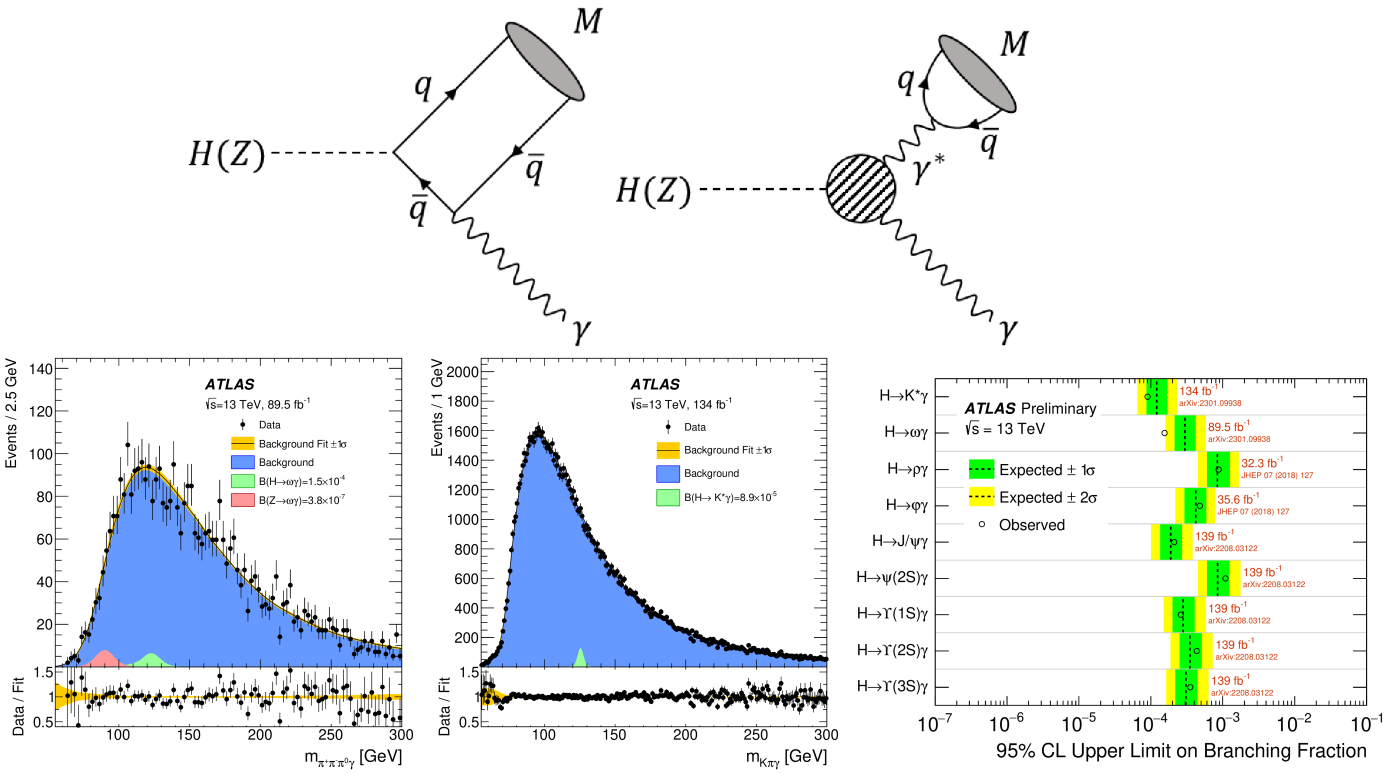

Figure 18. Upper: Feynman diagrams for the associated production of a meson and a photon in Higgs boson decays [24]. **Lower**: invariant masses of mesons and photons (**left** and **middle**) [24] and ATLAS public summary of the limits (**right**) [25]. Reproduced under the copyright permission from Elsevier (upper, lower left and middle) and under the CC-BY-4.0 license (lower right).

2.5. Lepton Flavor Violation (LFV)

Searches for LFV processes $H \to e\tau,\ \mu\tau$ led to limits on the Higgs boson branching fractions $\mathrm{BR}(H \to e\tau) < 0.20\%$ $(0.12\%$ exp.$)$ and $\mathrm{BR}(H \to \mu\tau) < 0.18\%$ $(0.09\%$ exp.$)$ at 95% CL. No measurement is compatible with LFV. Figure 19, upper left, shows an observed invariant-mass distribution along with the simulated $\mathrm{BR}(H \to e\tau)$ and $\mathrm{BR}(H \to \mu\tau)$ signals, which were observed and, in the SM, expected to be $\mathrm{BR}(H \to e\tau)$ and $\mathrm{BR}(H \to \mu\tau)$ results (Figure 19, upper right). Figure 19, lower, shows limits on these branching ratios set at 95% CL [26]. CMS experiment searches for LFV processes $H \to e\mu$ led to branching ratio limits 4.4 (4.7 exp.) $\times\ 10^{-5}$ at 95% CL [27]. An excess of events over the expected background is observed at an electron–muon invariant mass of approximately 146 GeV with a global (local) significance of 2.8 (3.8) s.d. Figure 20, left, shows the $e\mu$-invariant-mass distribution and Figure 20, middle, shows the resulting limits on the Higgs boson branching fractions $(H \to e\mu)$ at 95% CL [27]. The ATLAS Collaboration observed no significant signal, in agreement with the SM expectation (Figure 20, right) [28].

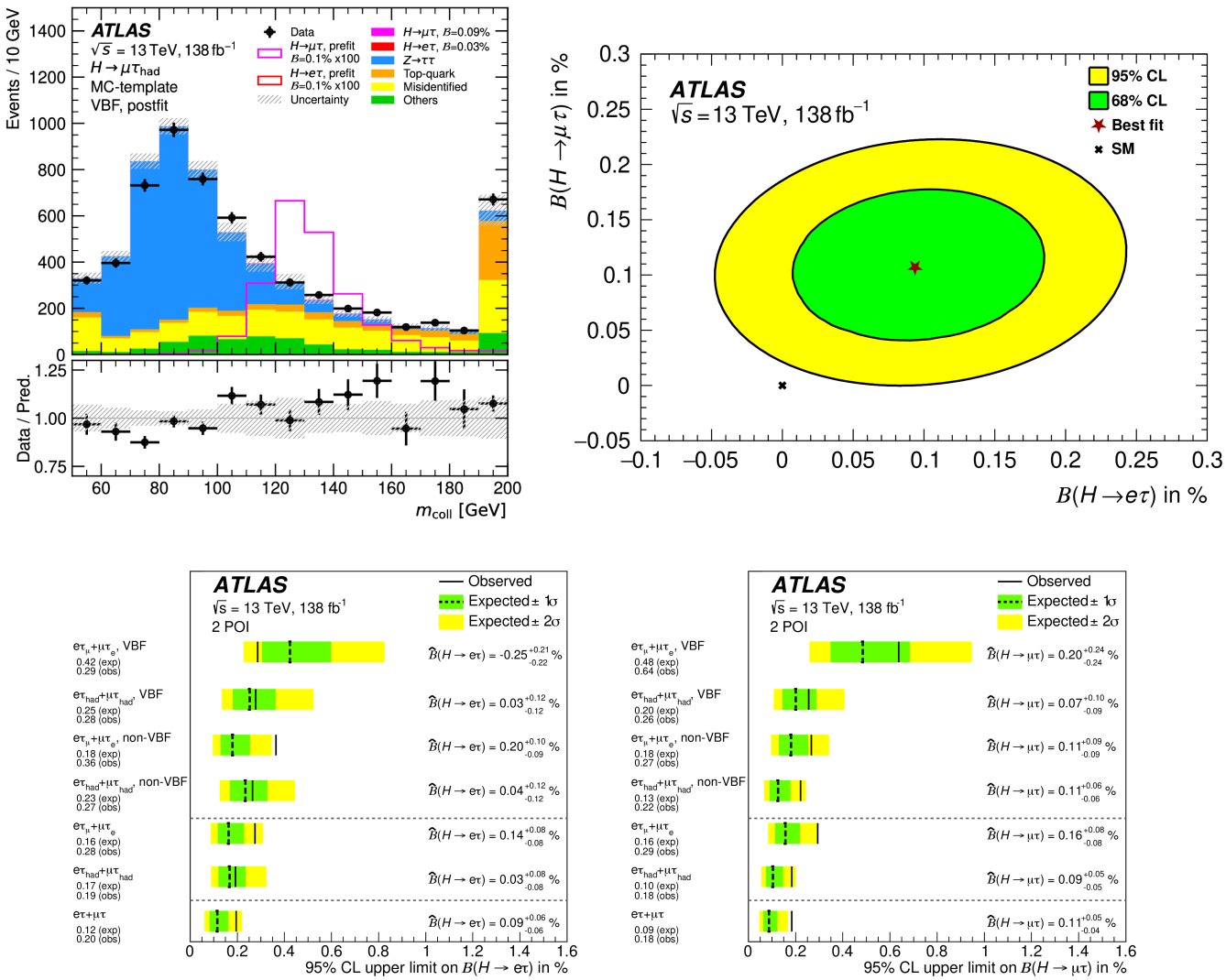

Figure 19. **Upper left**: invariant-mass distribution along with simulated BR($H \to e\tau$) and BR($H \to \mu\tau$) signals [26]. **Upper right**: observed and, in the SM, expected BR($H \to e\tau$) and BR($H \to \mu\tau$) results [26]. **Lower**: limits on BR($H \to e\tau$) and BR($H \to \mu\tau$) at 95% CL [26]. Reproduced under the copyright permission from Springer.

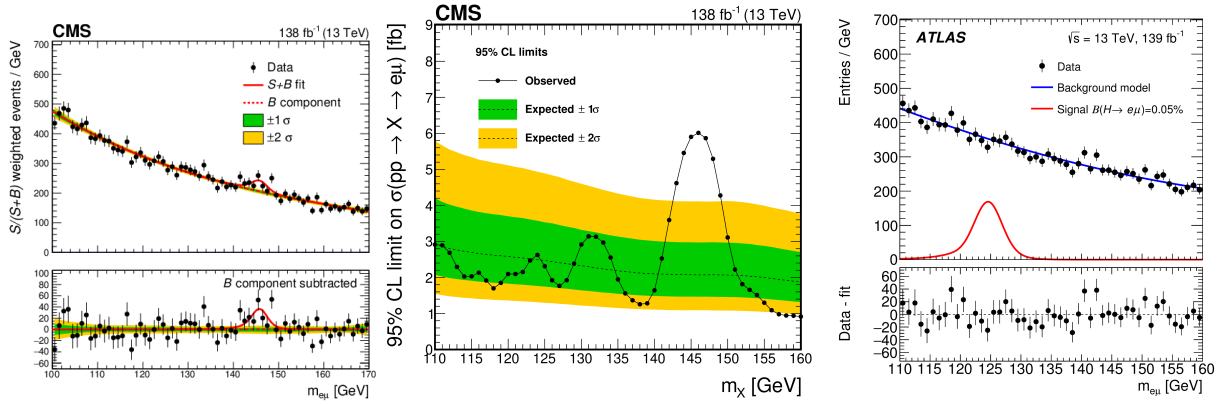

Figure 20. **Left**: CMS-experiment-observed $e\mu$-invariant-mass distribution [27]. **Middle**: CMS-experiment-measured limits BR($H \to e\mu$) at 95% CL [27]. **Right**: ATLAS-experiment-observed $e\mu$-invariant-mass distribution [28]. Reproduced under the copyright permission from the American Physical Society (left, middle) and Elsevier (right).

2.6. Invisible Decays

A strong motivation for the search for invisible Higgs boson decays is that this search can give insight into the hidden sectors of the Higgs field [29]. Direct searches were made by the ATLAS Collaboration for Higgs bosons that decay into invisible particles (leading to missing energy) [30]. Signatures could be jet+E_T^{miss}, VBF+E_T^{miss}+photon, tt+E_{rmT}^{miss}, $Z(\ell\ell)$+E_T^{miss}, and VBF+E_T^{miss} final states. is the missing transverse momentum. The photon could arise from ISR QED radiation and jets from QCD radiation. No indication of a signal has been found, and a limit is set on the BR$(H \to inv) < 0.107$ $(0.077$ exp.$)$ at 95% CL, assuming a SM production cross-section [30] (Figure 21, left); here "inv" denotes the above listed final states of invisible particles. Figure 21, right, shows details of the limit setting and an interpretation as limits on a weakly interacting massive particle (WIMP) [30]. Results by the CMS Collaboration were obtained in the ttH search BR$(H \to inv) < 0.47$ (0.40) at 95% CL, and in the combined ggH, VBF, VH, and ttH analyses $(H \to inv) < 0.15$ (0.08) at 95% CL [31] (Figure 22, right). Details on the limit setting and an interpretation as limits on a WIMP are shown in Figure 22, right [31]. For light mass, dark matter (DM) candidates in the range of 0.1 GeV and $m_H/2$ (Higgs mass) model-dependent exclusion limits are found to complement direct-detection experiments.

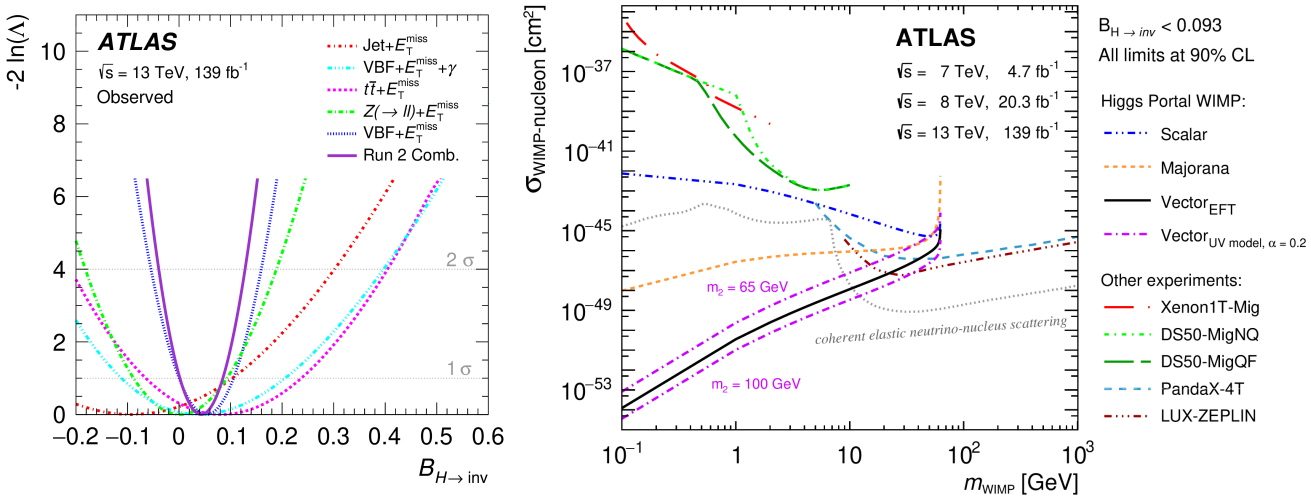

Figure 21. Left: twice the negative logarithmic profile likelihood ratio as a function of BR$(H \to inv)$ decays into invisible particles [30]. **Right**: upper limits on the interaction cross-section of WIMP dark matter candidates with nucleons [30]. Reproduced under the copyright permission from Elsevier.

2.7. Dark Photons

There is strong astrophysical evidence suggesting the existence of DM [32]. The dark and visible physics sectors may interact through a portal, offering a potential experimental signature [33], including massive dark photons with energy $E_\gamma = m_{H/2}$ in the Higgs center-of-mass. Figure 23, left, shows the Feynman production diagram and Figure 23, right, shows the obtained upper limits on the Higgs boson decay branching ratios to $H \to \gamma\gamma_D$ [34], where the subscript "D" indicates the DM photon.

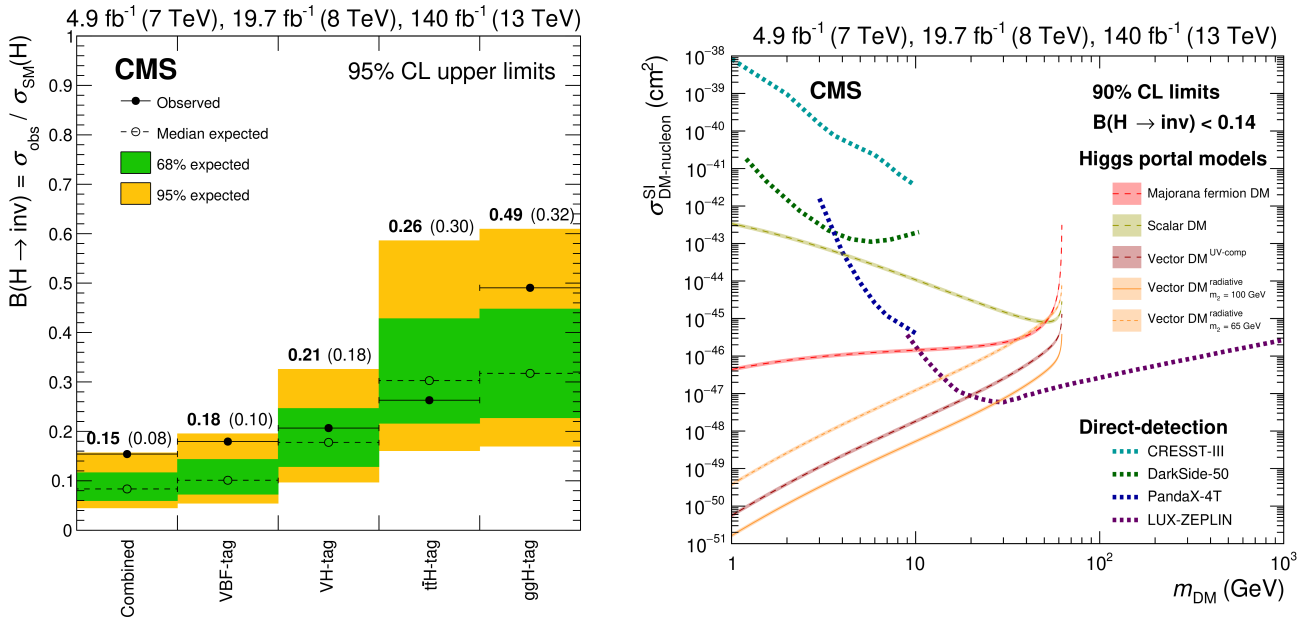

Figure 22. Left: upper limits and Higgs boson decay branching ratios into invisible particles [31]. **Right**: upper limits on interaction cross-sections of dark matter (DM) candidates [31]. Reproduced under the copyright permission from Springer.

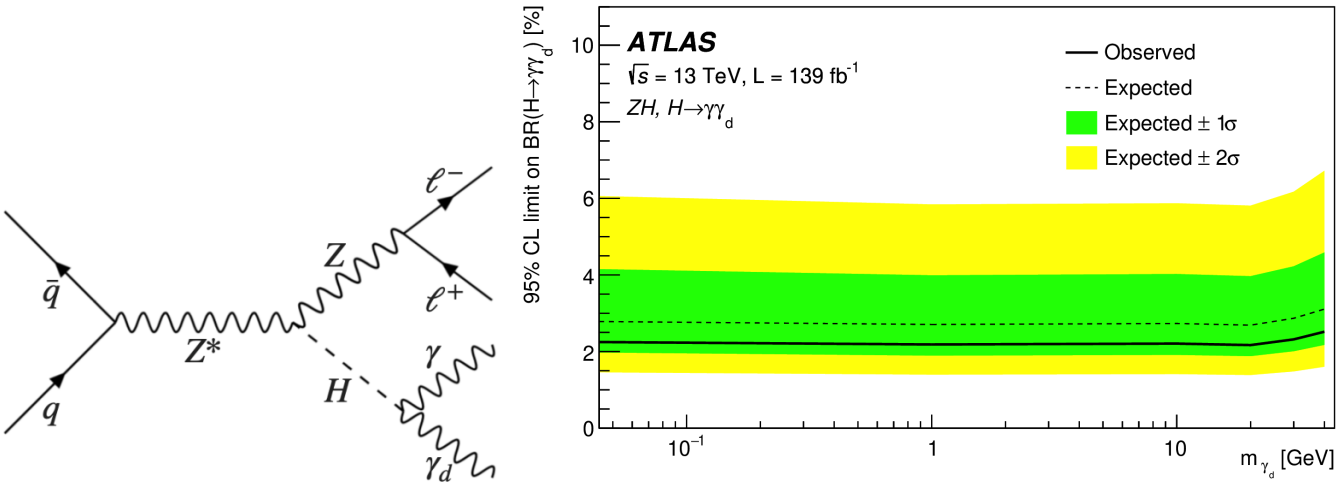

Figure 23. Left: dark photon production Feynman diagram. **Right**: upper limits on the Higgs boson decay branching ratios to $H \to \gamma\gamma_D$ [34]. Reproduced under the copyright permission from Springer.

2.8. Exotic Scalar Particles

An elegant solution to the strong CP problem by Roberto Peccei and Helen Quinn [35] is the introduction of a spontaneously broken U(1) symmetry leading to new light pseudoscalar particles—the axions—that couple very weakly to photons. At LHC, a search for the production of axion-like pseudoscalar particles in the decay $H \to Za$ with $Z \to \ell\ell$, where $\ell = e, \mu$ and $a \to \gamma\gamma$, is reported. Figure 24 shows simulated $ee\gamma\gamma$ and $\mu\mu\gamma\gamma$ signals (Figure 24, upper middle and upper right), efficiency times acceptance (Figure 24, lower left and lower middle), and limits on the Higgs boson decay branching fraction (Figure 24, lower right). Limits on models involving axion-like particles, formulated as an effective field theory, were also reported in Ref. [36].

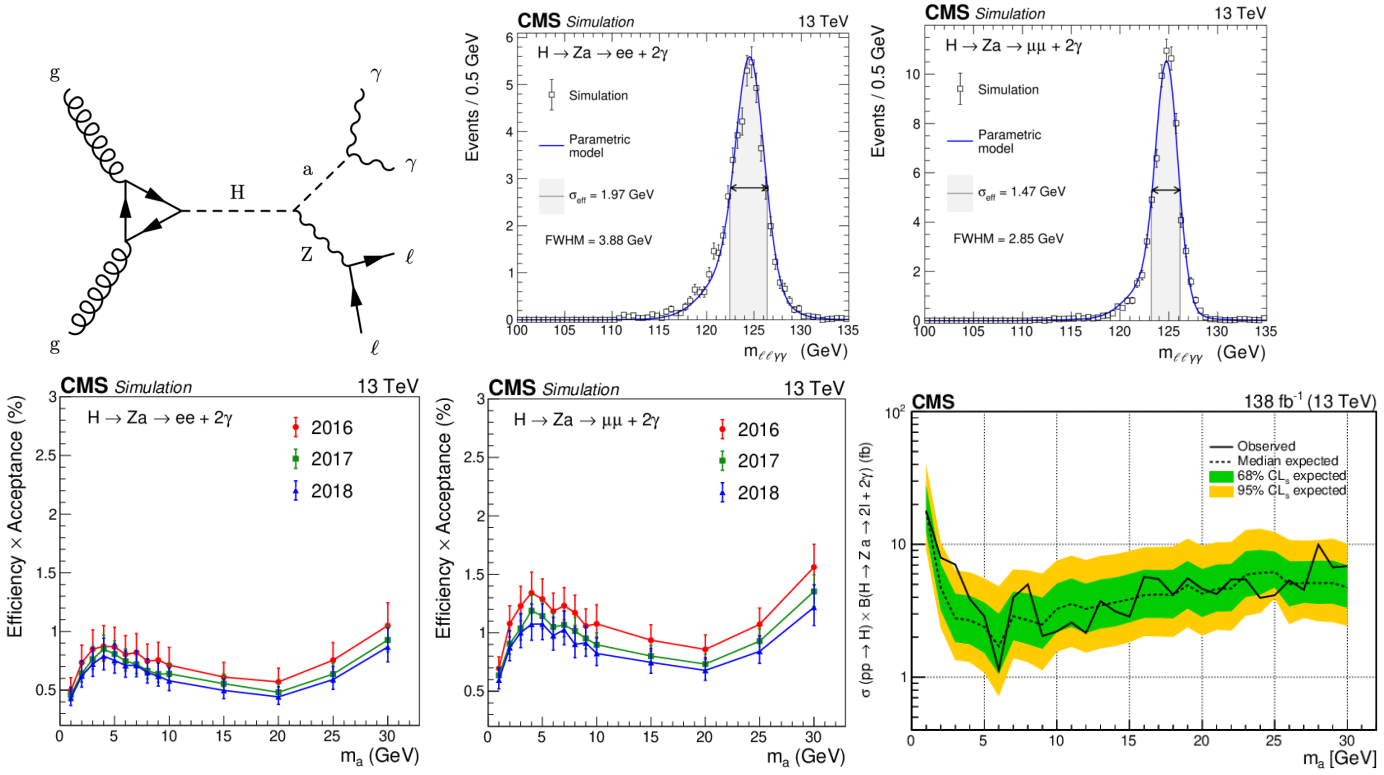

Figure 24. Upper left: Feynman diagram for $H \to Za$ with $Z \to \ell\ell$, where $\ell = e, \mu$ and $a \to \gamma\gamma$. **Upper middle** and **right**: simulated $ee\gamma\gamma$ and $\mu\mu\gamma\gamma$ signals [36]. **Lower**: efficiency times acceptance (**left** and **middle**) and limits on the Higgs boson decay branching fraction (**right**) [36]. Reproduced under the copyright permission from Elsevier.

In models with two Higgs doublets extended with a scalar singlet (2HDM+S), the decay $H \to aa \to \mu\mu bb$ and $\tau\tau bb$ may exist. Figure 25, left, shows limits on the Higgs boson decay branching ratio $H \to aa \to \mu\mu bb, \tau\tau bb$ and Figure 25, right, the limits in the parameter space $(m_a, \tan\beta)$ [37].

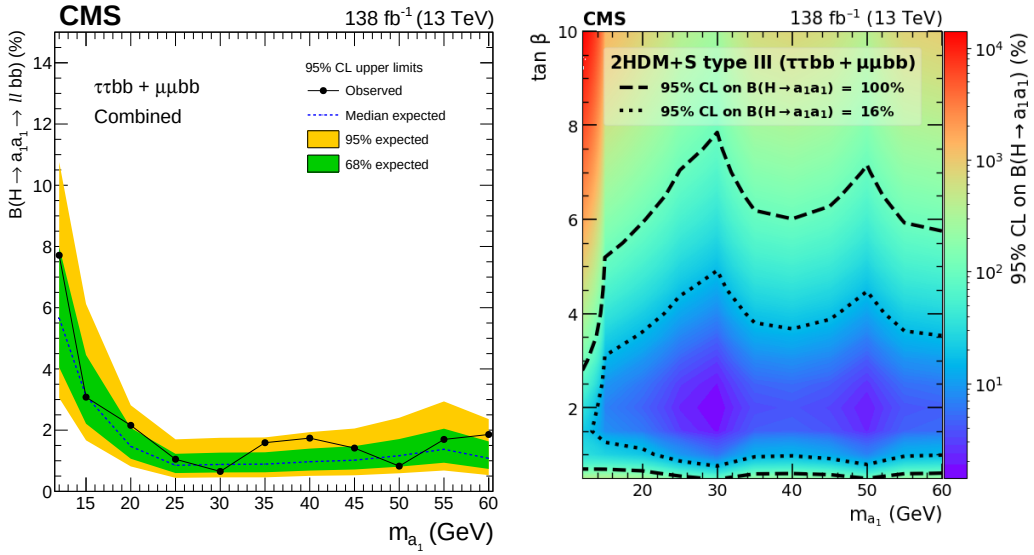

Figure 25. Left: limits on the Higgs boson decay branching ratio $H \to aa \to \mu\mu bb, \tau\tau bb$ [37]. **Right**: limits in the parameter space $(m_a, \tan\beta)$ [37]. Reproduced under the copyright permission from Springer.

In the 2HDM+S framework, low-mass di-muons are predicted $a \to \mu\mu$. For setting limits, $\tan\beta = 0.5$ is assumed, and $\sigma(pp \to a) = sin^2(\Theta_H) \times B \times A$, where $B = BR(a \to \mu\mu)$, with acceptance A. No significant excess of events above the expectation from the SM background was observed [38], and the resulting limits are compared to previous limits from LHCb [39] and BaBar [40] experiments. Figure 26, left, compares the observed and the expected limits on the production cross-section times branching ratio times acceptance and Figure 26, right, shows the limit on the mixing angle $\sin\Theta_H$ [38].

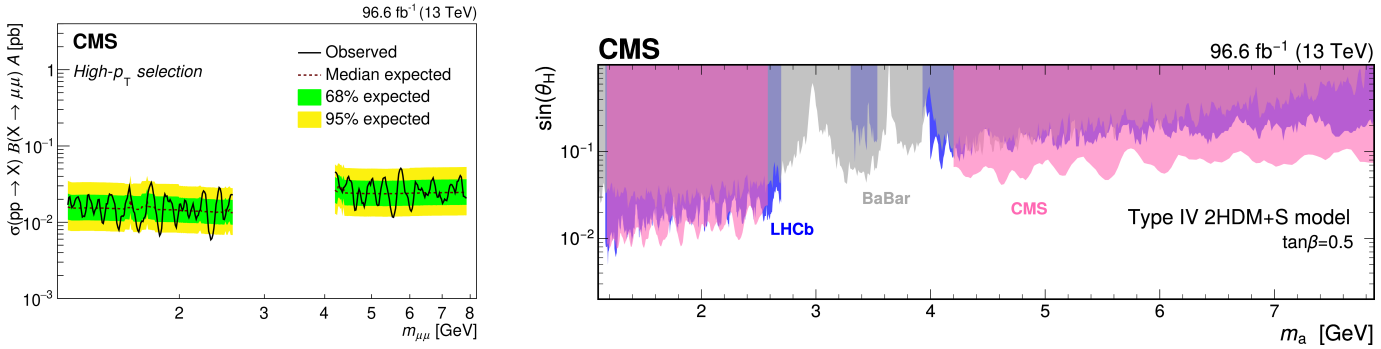

Figure 26. Left: observed versus expected limits at 95% CL on the production cross-section times branching ratio times acceptance [38]. **Right**: limits at 90% CL on the mixing angle $\sin\Theta_H$ [38] compared to previous limits from LHCb [39] and BaBar [40] experiments. Reproduced under the copyright permission from Springer.

Low-mass spin-0 particles can decay promptly to a closely separated photon pair that is reconstructed as a single photon-like object, $H \to AA \to 4\gamma$. Figure 27, left, compares the number of events for data, the simulated signal and background and Figure 27, right, represents the resulting limits on the branching ratio BR$(H \to AA \to 4\gamma)$ [41].

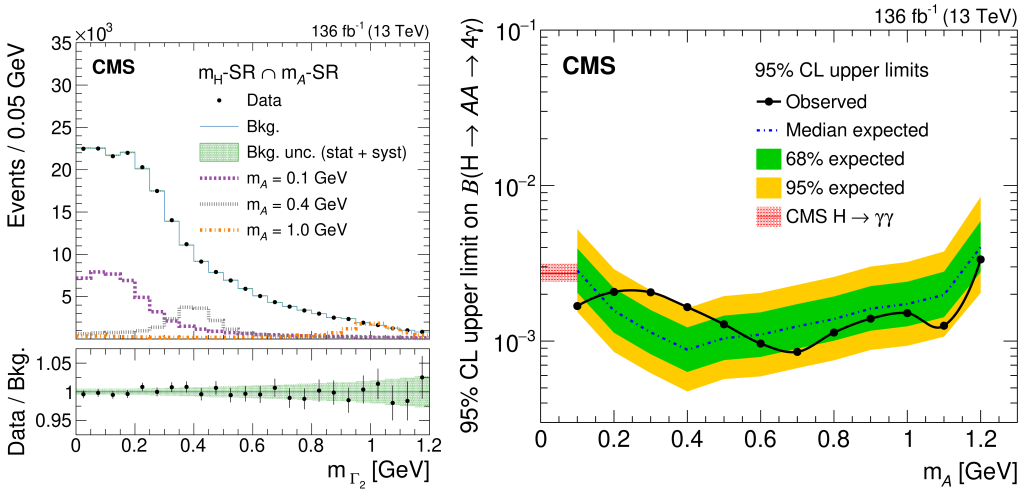

Figure 27. Left: number of events for data versus the simulated signal and background [41]. **Right**: limits on the Higgs boson decay branching ratio BR$(H \to AA \to 4\gamma)$ [41]. Reproduced under the copyright permission from the American Physical Society.

3. Enhanced Production Modes

BSM physics may enhance (or decrease) the production rates of Higgs bosons. This may lead to the observation of a SM reaction, where the SM predicts a rate below the sensitivity reach. Here, the measurements of tH (ttH) and HH signals are discussed.

3.1. Single Top Higgs

The expected production rate of ttH and tH events with $H \to bb$ is different for CP-even and CP-odd ttH and tH signals and, in particular, for the tH enhancement in the production BSM for the CP-odd case. Figure 28 shows a tH production Feynman diagram and Table 6 gives the expected number of ttH and tH events for CP-even and CP-odd signals. The measured mixing angle between CP-even and CP-odd couplings is compatible with zero: $\alpha = 11^{+52}_{-72}$ degrees [42].

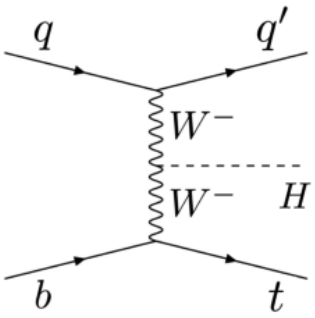

Figure 28. tH production Feynman diagram.

Table 6. ATLAS expected number of ttH and tH events for CP-even (0°) and CP-odd (90°) signals. The signals are given for unity coupling strength and post-fit coupling strength 0.84 [42].

	$\mathbf{CR}^{5j,\geq 4b}_{\mathbf{lo}}$	$\mathbf{CR}^{5j,\geq 4b}_{\mathbf{hi}}$	$\mathbf{CR}^{\geq 6j,\geq 4b}_{\mathbf{1}}$	$\mathbf{CR}^{\geq 6j,\geq 4b}_{\mathbf{2}}$	$\mathbf{SR}^{\geq 6j,\geq 4b}$	$\mathbf{SR}_{\mathbf{boosted}}$
$t\bar{t}H(1,0°)$	60 ± 9	63 ± 10	78 ± 11	139 ± 18	173 ± 26	46 ± 6
$tH(1,0°)$	3.5 ± 0.5	3.8 ± 0.6	3.3 ± 0.6	2.3 ± 0.6	1.3 ± 0.4	1.9 ± 0.4
$t\bar{t}H(1,90°)$	28 ± 6	28 ± 6	45 ± 11	61 ± 12	68 ± 16	45 ± 6
$tH(1,90°)$	19.0 ± 2.8	19.4 ± 3.1	17.4 ± 3.1	13.1 ± 3.5	10 ± 4	29 ± 6
$t\bar{t}H(0.84,11°)$	40 ± 30	41 ± 31	50 ± 40	90 ± 70	110 ± 80	30 ± 22
$tH(0.84,11°)$	3 ± 4	3.9 ± 1.9	3.1 ± 1.9	1.9 ± 0.8	1.3 ± 1.7	3 ± 5
$t\bar{t}$ + $\geq 1b$	1530 ± 80	1090 ± 60	4300 ± 120	2220 ± 120	1110 ± 110	335 ± 30
$t\bar{t}$ + $\geq 1c$	650 ± 50	96 ± 11	950 ± 80	450 ± 40	153 ± 15	196 ± 22
$t\bar{t}$ + light	280 ± 40	28 ± 8	230 ± 60	117 ± 26	32 ± 11	76 ± 15
Other	173 ± 30	99 ± 20	320 ± 50	159 ± 21	83 ± 11	60 ± 11
Total	2690 ± 50	1350 ± 40	5870 ± 80	3040 ± 70	1500 ± 50	701 ± 31
Data	2696	1363	5837	3090	1470	699

The single top and Higgs boson production: tH, where $H \to WW/ZZ/\tau\tau$ and $H \to bb$, is combined with the production ttH $(H \to \gamma\gamma)$ [43]. Since the production is sensitive to the absolute values of the top quark Yukawa coupling, the Higgs boson coupling to vector bosons, $g(HVV)$, and, uniquely, their relative sign, are studied. The data favor $\kappa_t = 1.0$ over $\kappa_t = -1.0$ for the coupling modifier by more than 1.5 s.d. Figure 29, left, shows a distribution of data along with the simulated background and signal, for $\kappa_t = 1.0$ and $\kappa_V = 1.0$, in addition to the measured likelihood as a function of κ_t (Figure 29, right).

The single top and Higgs boson tH production has also been analyzed with combined $H \to WW/ZZ/\tau\tau/bb/\gamma\gamma$ decays. The ttH normalization is kept fixed in the fit to the SM expectation, while the tH signal strength is allowed to float. Discrepancies between observed and expected limits at $\kappa_t = 0.0$ are caused by the predicted ttH vanishing while the data favor even larger than expected yields for ttH production. Figure 30, left, compares the measured tH and ttH couplings with those from the SM expectations and Figure 30, right, shows the measured likelihood as a function of κ_t [44]. An upper limit at 95% CL on the tH production rate of 14.6 times the SM expectation is observed, with an expectation of $19.3^{+9.2}_{-6.0}$ [44].

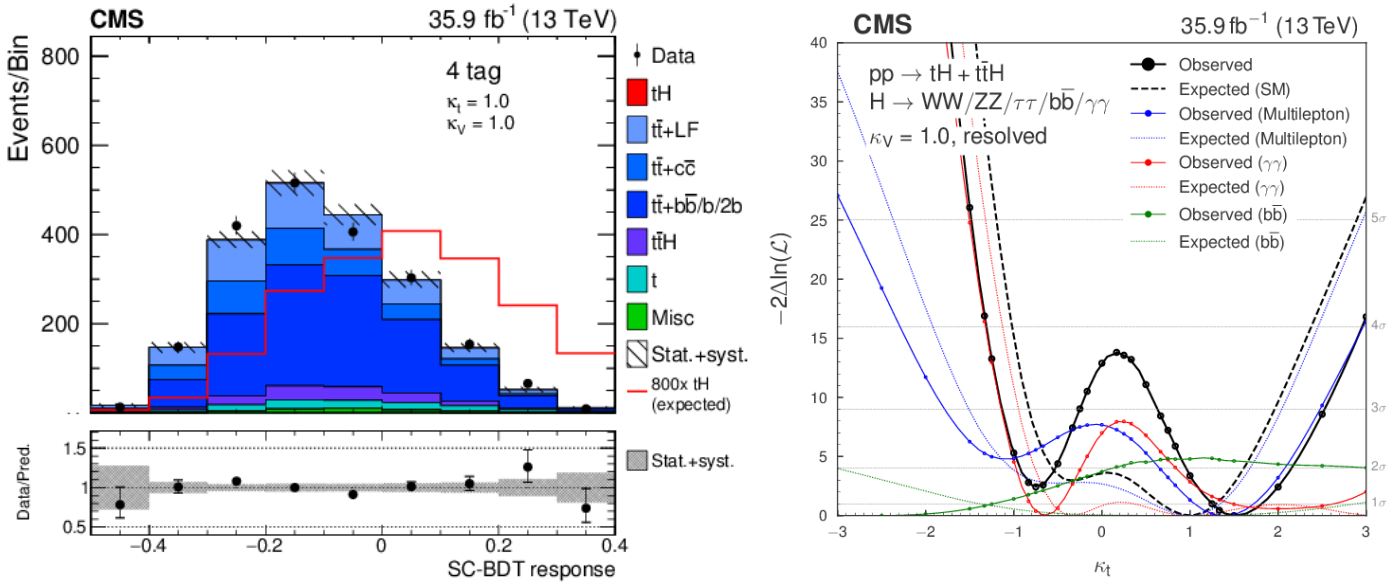

Figure 29. Left: signal classification BDT (SC-BDT) for data, simulated background, and tH signal for $\kappa_t = 1.0$ [43]. **Right**: measured likelihood as a function of κ_t [43]. Reproduced under the copyright permission from the American Physical Society.

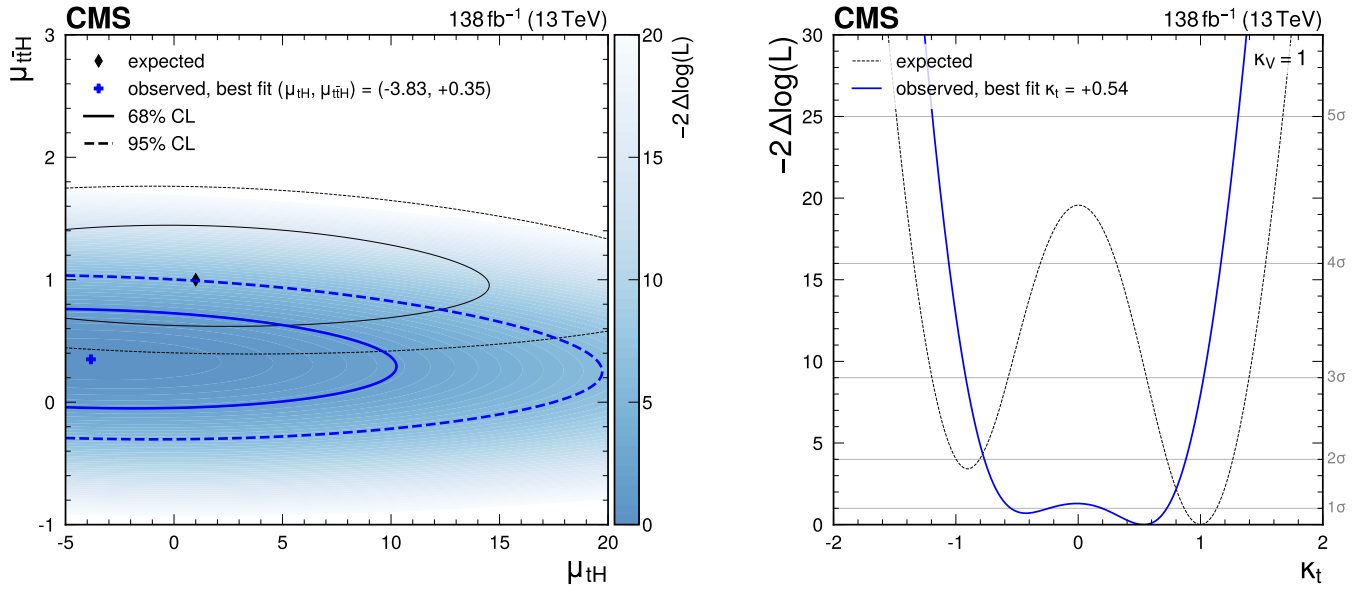

Figure 30. Left: measured tH and ttH signal strengths compared to the SM expectations [44]. **Right**: measured likelihood as a function of κ_t. The SM value $\kappa_t = 1.0$ is outside the two standard deviation confidence interval [44]. Reproduced under the CC-BY-4.0 license.

3.2. Di-Higgs, κ_λ, κ_{2V}

The parameter κ_λ is the HHH trilinear coupling modifier. Its value is left free in the fit to the recorded data, and in the SM, $\kappa_\lambda = 1$. Upper limits are set on the production signal strength, including the data from several final states $HH \to bbbb, bb\tau\tau, bb\gamma\gamma$ at 2.4 (2.9 exp.) and on the coupling modifier $-0.4 < \kappa_\lambda < 6.3$ at 95% CL [45,46]. Figure 31, upper, shows the dominant Feynman diagrams of HH production, while Figure 31, lower left, shows the upper limits on the HH signal strength with respect to the SM ggF+VBF induced production, and Figure 31, lower right, the upper limits on the cross-section of the ggF and VBF productions of HH [45].

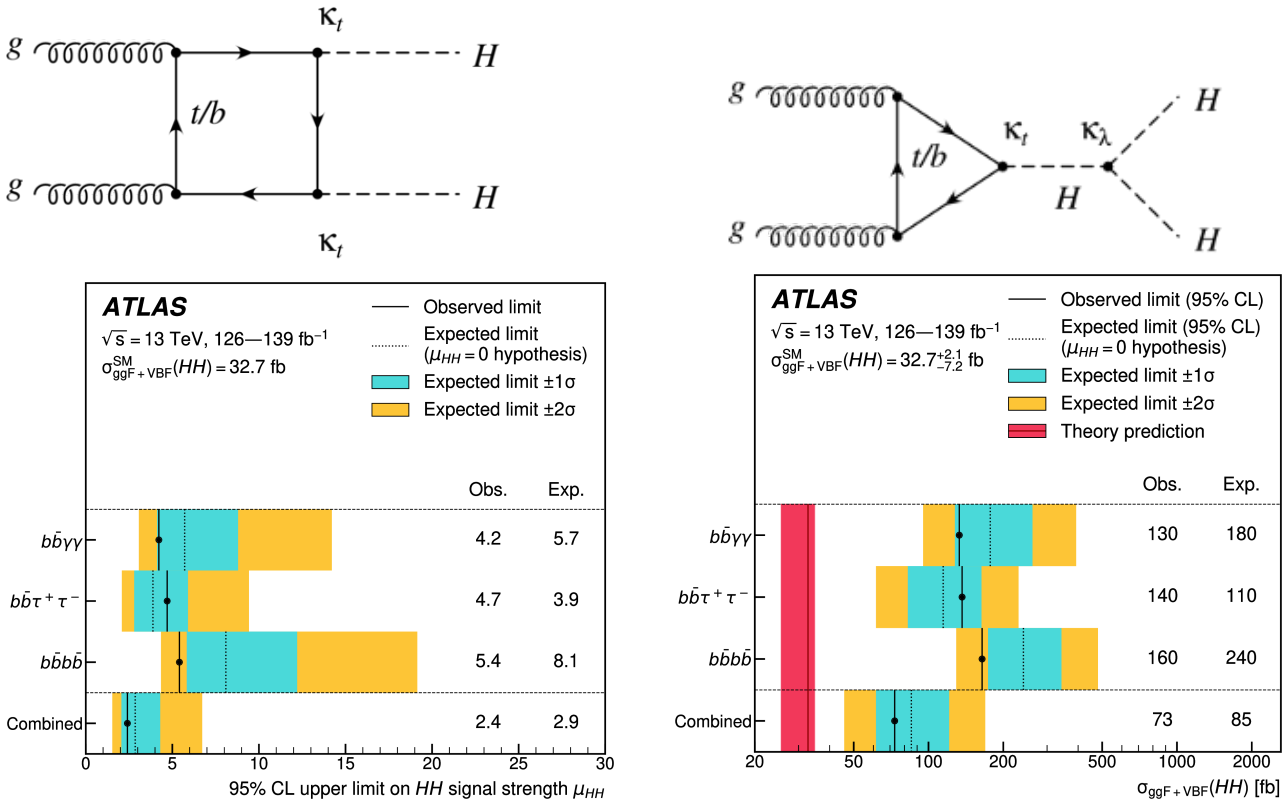

Figure 31. Upper: Feynman diagrams of HH production. **Lower**: upper limits (**left**) on the HH signal strength with respect to the SM ggF+VBF induced production and (**right**) on the cross-section of the ggF and VBF productions of HH [45]. Reproduced under the copyright permission from Elsevier.

Observed and expected limits on the HHH coupling modifier are set at 95% CL based on only the $bbbb$ final state and considering both κ_λ in $[-3.5, 11.3]$ ($[-5.4, 11.4]$ exp.) and κ_{2V} in $[-0.0, 2.1]$ ($[-0.1, 2.1]$ exp.) intervals. Limits are also set on the production cross-section in seven Higgs effective field theory benchmark scenarios [47]. Figure 32, upper left, shows a Feynman diagram for $VVHH$ scattering. Figure 32, upper middle and upper right, shows the data compared to simulated background and HH signal and the limits on the κ_λ and κ_{2V} plane, respectively. Figure 32, lower left and right, shows the limits on the ggF+VBF HH production cross-sections as a function of κ_λ and κ_{2V}, respectively. The SM predictions $\kappa_\lambda = 1$ and $\kappa_{2V} = 1$ are in the measured ranges.

The production of $HH \to bbWW$ is constrained to be less than 14 (18 exp.) times the SM expectation at 95% CL [48]. In the Higgs effective field theory (HEFT) parameterization, limits are set for benchmark scenarios. In addition, the production $HH \to bbZZ, multilepton, bb\gamma\gamma, bb\tau\tau, bbbb$ is constrained at 3.4 (2.5 exp.) times the SM expectation at 95% CL [12]. Figure 33, left, shows limits on the HH production cross-section for benchmark scenarios [48], in agreement with the expectations, along with the combined limits on the HH production cross-section compared to the SM expectation in Figure 33, right [12].

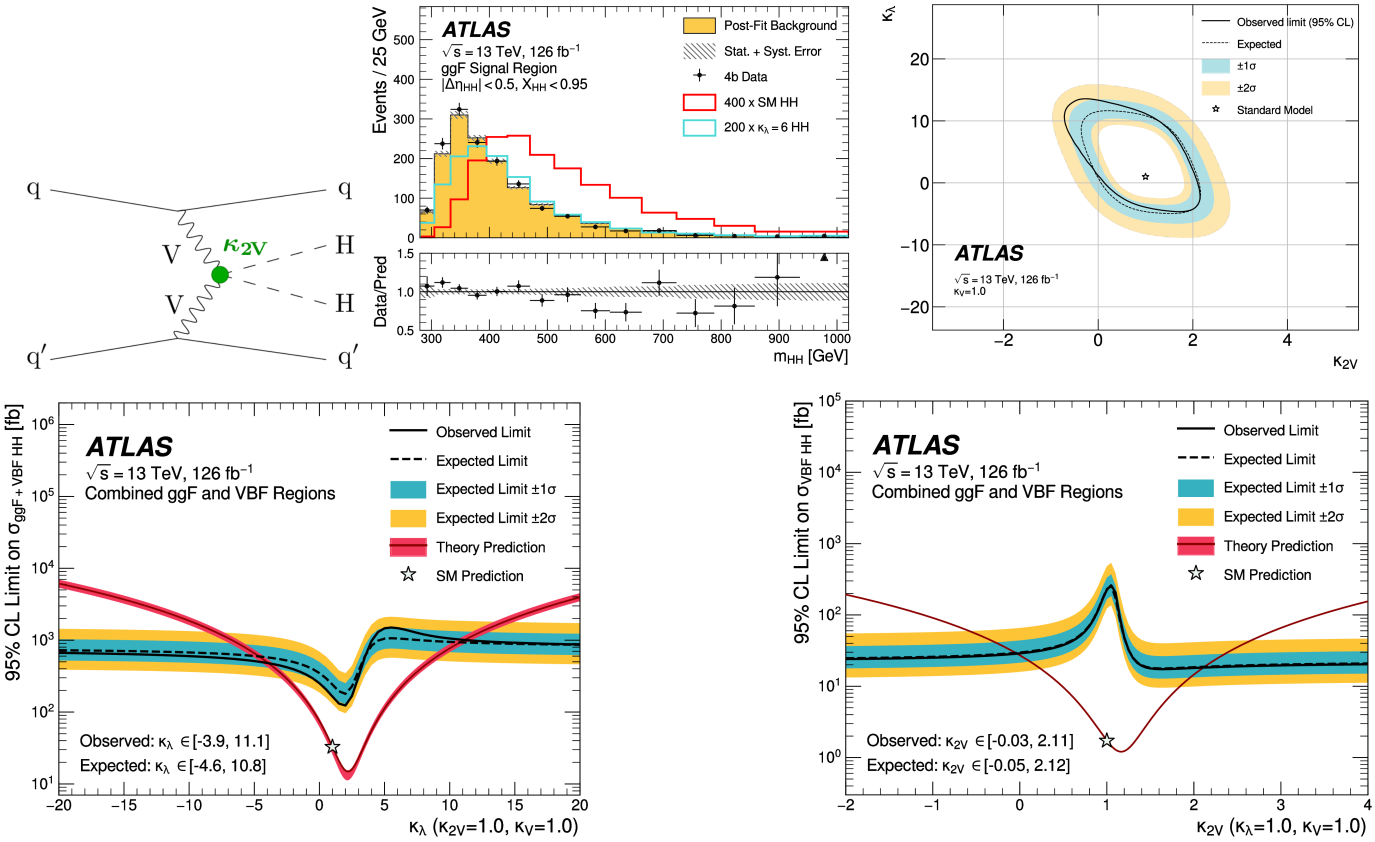

Figure 32. Upper left: Feynman diagram for $VVHH$ scattering. **Upper middle**: data, simulated background, and HH signal [47]. **Upper right**: limits on the κ_λ and κ_{2V} plane [47]. **Lower**: limits on the VBF and ggF+VBF HH production cross-sections as a function of (**left**) κ_λ and (**right**) κ_{2V} [47]. See text for details. Reproduced under the copyright permission from the American Physical Society.

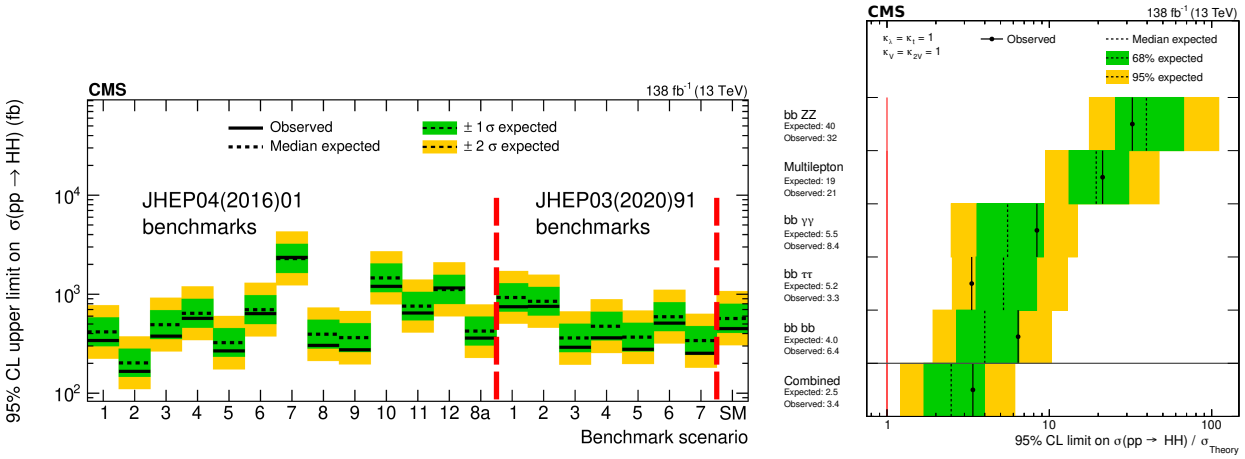

Figure 33. Left: limits on the HH production cross-section for benchmark JEHP03, JHEP04 and SM scenarios [48]. **Right**: individual and combined limits on the HH production cross-section compared to the SM expectation [12]. Reproduced under the copyright permission from Springer (left) and Springer Nature (right).

An overview of the $\kappa_\lambda = 1.7^{+2.8}_{-1.7}$ and $\kappa_{2V} = 1.0^{+0.2}_{-0.2}$ measurements is given in Figure 34 [49], left and right, respectively. $\kappa_{2V} = 0$ is excluded with 6.6 s.d., and this establishes the existence of the quartic coupling VVHH, assuming $\kappa_\lambda = 1$. Values of κ_λ outside the interval $-1.2 < \kappa_\lambda < 7.5$ are excluded at 95% CL [50].

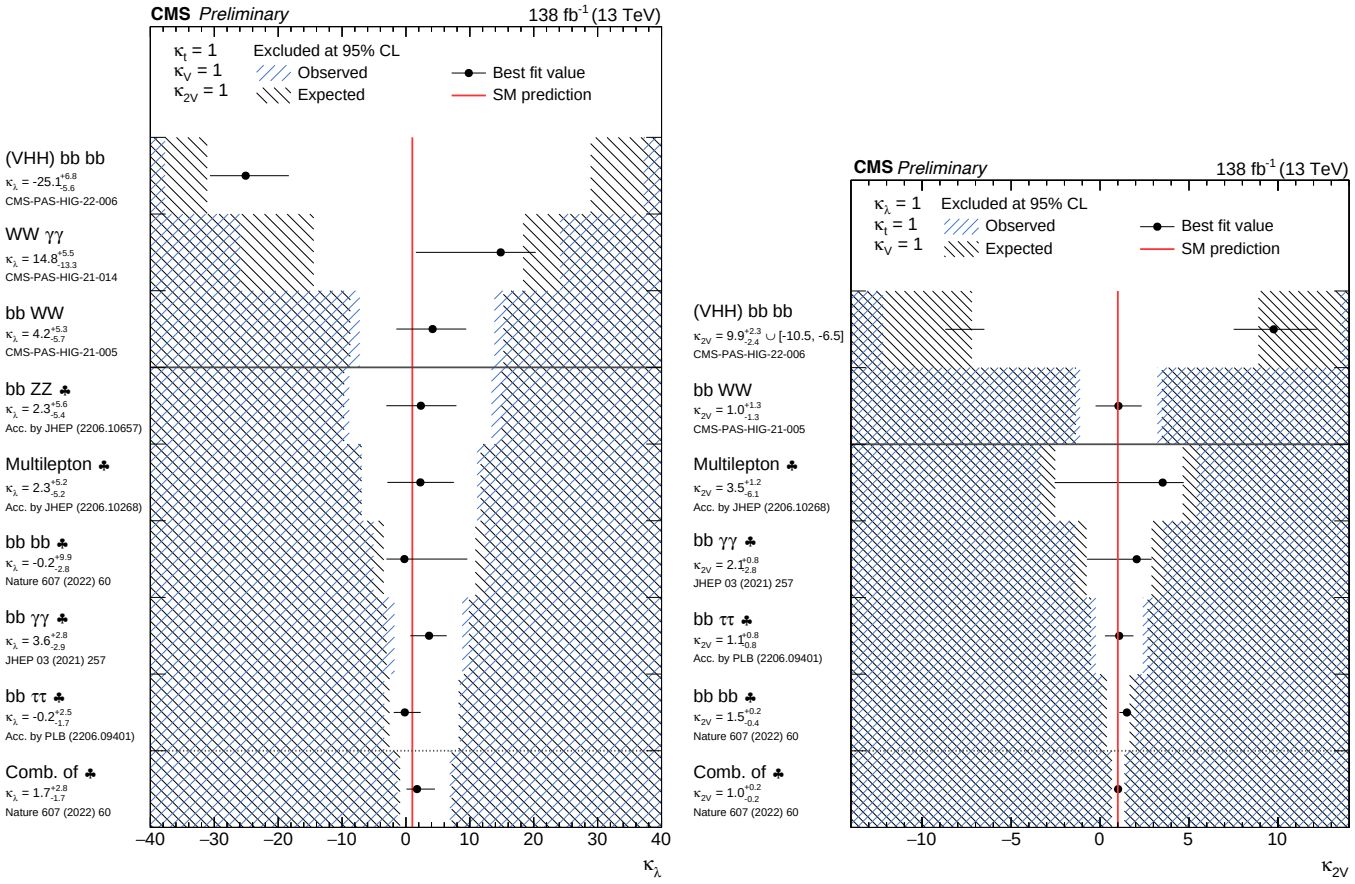

Figure 34. κ_λ (**left**) and κ_{2V} (**right**) measurements [49] (CMS public results). Reproduced under the CC-BY-4.0 license.

4. Higgs Boson Resonances

4.1. $X \to SH \to WW\tau\tau, ZZ\tau\tau$

A search for a new heavy scalar X decaying into a Higgs boson and a new scalar singlet S, $X \to SH$, was performed in the mass range 500 GeV–1500 GeV for X and in the mass range 200 GeV–500 GeV for S. The Higgs boson decays into a pair of τ leptons, and the S decays into pairs WW and ZZ, which subsequently decay into light leptons. No signal has been observed [51]. Figure 35, left, shows a Feynman diagram for the SH production, while Figure 35, middle and right, shows simulated background plus SH signal as a function of the BDT score for WW and ZZ, respectively.

4.2. $X \to YH \to bbbb$

The search for the process $X \to YH \to bbbb$ has been performed for the mass ranges 0.9 TeV–4.0 TeV for X and 60 GeV–600 GeV for Y scalars [52]. For the interpretations, there are the two-real-scalar-singlet extension of the SM (TRSM) and the next-to-minimal model (NMSSM). Figure 36 [52] shows the invariant mass, M_{JJ}, the distribution of the two leading-p_T jets in the event for the data, the simulated background and $X \to YH \to bbbb$ signals (Figure 36, left), and the observed exclusion limits in the mass parameter space M_X and M_Y at 95% CL (Figure 36, right). Both Y and H are reconstructed as Lorentz-boosted single large-area substructure jets J.

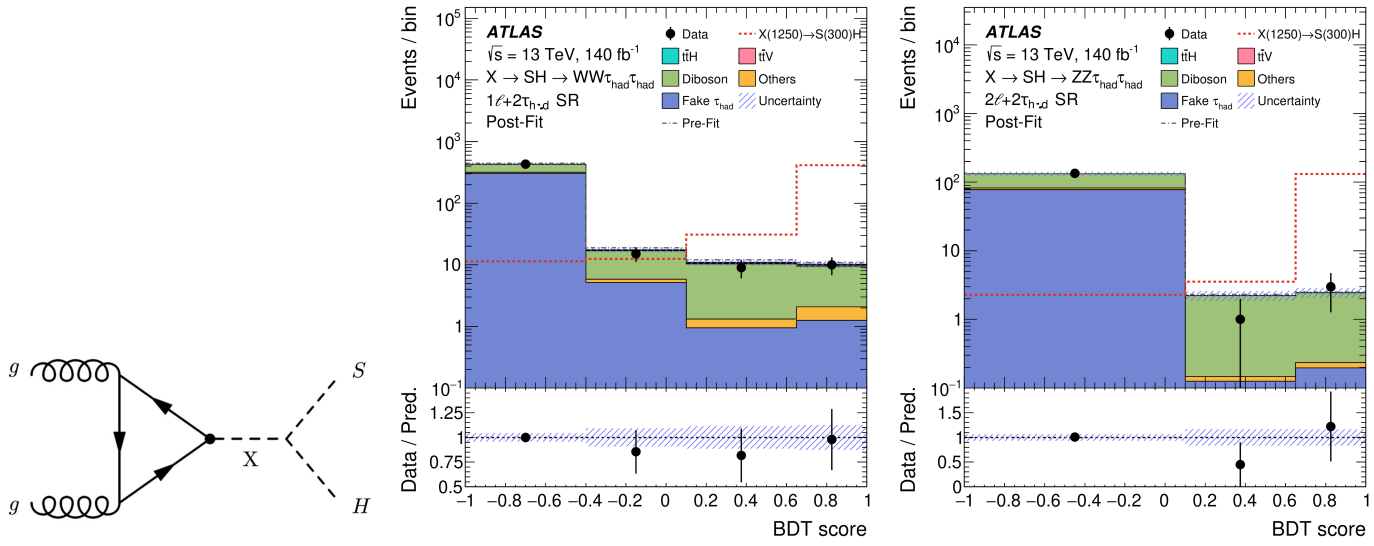

Figure 35. Feynman diagram for the SH production (**left**); data, simulated background, and SH signal as a function of the BDT score for $X \to SH \to WW\tau\tau$ (**middle**) and $X \to SH \to ZZ\tau\tau$ (**right**) [51]. Reproduced under the copyright permission from Springer.

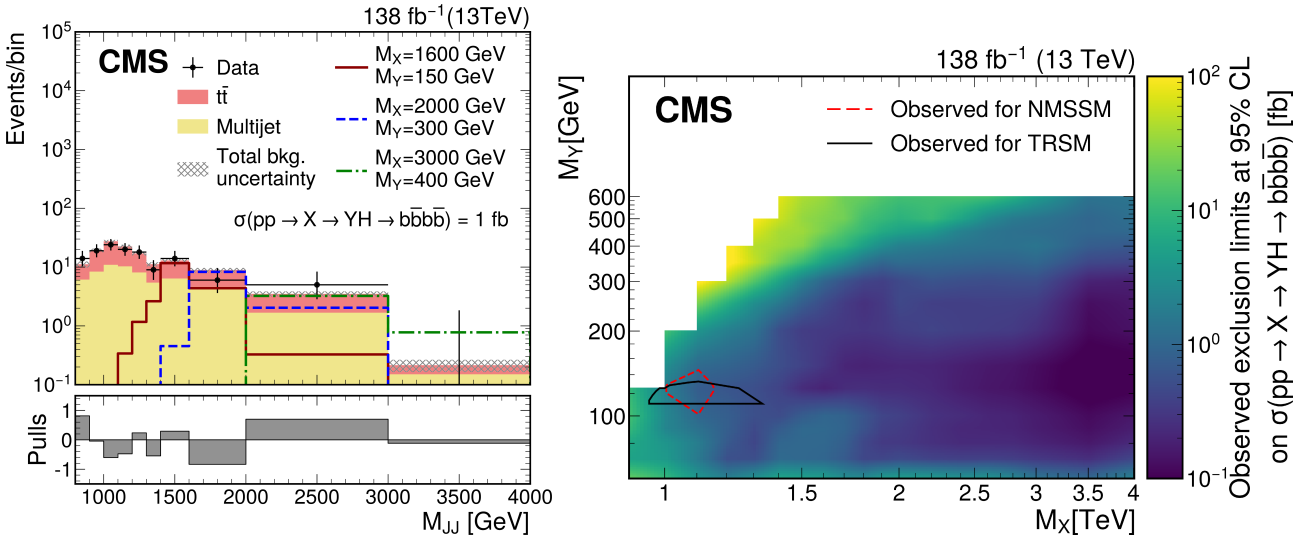

Figure 36. Left: data, simulated background, and $X \to YH \to bbbb$ signals [52]. Both Y and H are reconstructed as Lorentz-boosted single large-area substructure jets J. **Right**: observed exclusion limits in the mass parameter space M_X and M_Y at 95% CL [52]. Reproduced under the copyright permission from Elsevier.

4.3. $X \to HH$

A summary of $X \to HH$ resonance searches and resulting limits are given in Figure 37 [53,54]. The ATLAS experiment sets upper limits on the production cross-section of a heavy scalar resonance decaying to two SM Higgs bosons at 95% CL between 0.96 and 600 fb (1.2 and 390 fb) in observation (expectation) [53], while CMS experiment sets the limit between 0.1 and 150 fb, depending on the X mass [54].

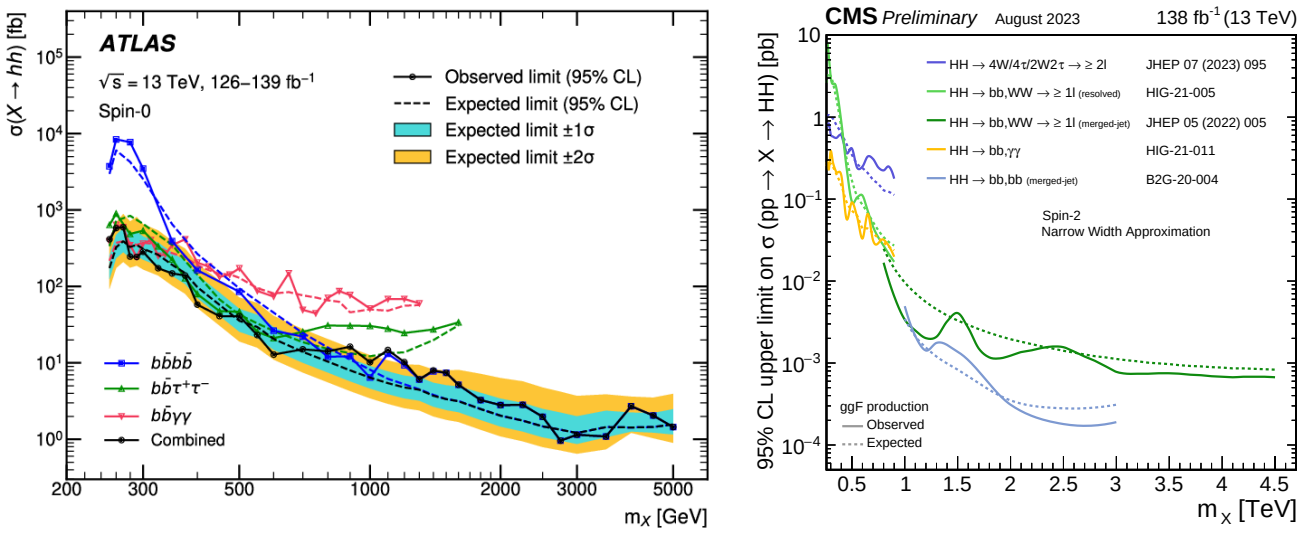

Figure 37. Summary of $X \to HH$ resonance searches and resulting limits by the (**left**) ATLAS [53] and (**right**) CMS [54] experiments. Reproduced under the copyright permission from the American Physical Society (left) and under the CC-BY-4.0 license (CMS public results; right).

5. Additional Neutral Higgs Bosons

5.1. SM-like Higgs Boson in the 70 GeV to 110 GeV Mass Range $H \to \gamma\gamma$ Decay

The search for a SM-like Higgs boson in the 70 GeV to 110 GeV mass range $H \to \gamma\gamma$ was performed in 36.3 fb^{-1}, 41.5 fb^{-1} and 54.4 fb^{-1} data from 2016, 2017, and 2018 data samples, respectively. The observed upper limit for the combined dataset ranged from 73 fb to 15 fb [55]. An excess with 2.9 s.d. local (1.3 s.d. global) significance was observed for a mass hypothesis of 95.4 GeV. Figure 38 shows the di-photon invariant mass distribution (Figure 38, left), resulting limits on the SM Higgs boson production times decay branching ratio into di-photons (Figure 38, middle), and local probability p-values as a function of the Higgs boson mass (Figure 38, right) [55]. No significant excess was observed by the ATLAS Collaboration [56] with 1.7 s.d. at 95.4 GeV. Earlier, an excess in combined LEP data was noted in the mass range of 90 GeV–100 GeV [57] of 2.3 s.d.; such an excess may be accommodated in a MSSM parameter scan [58].

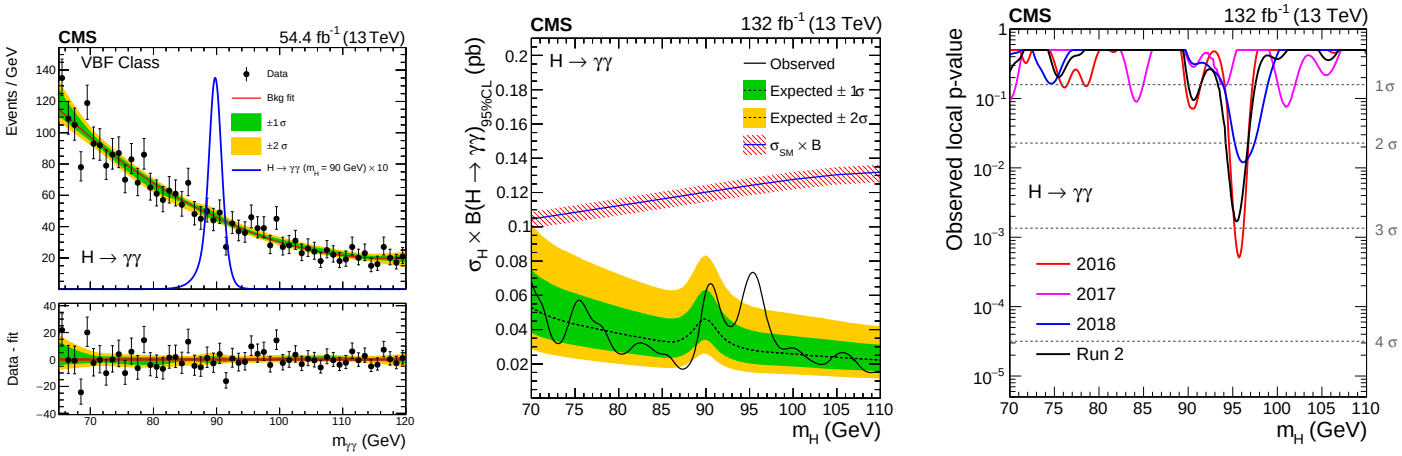

Figure 38. Left: di-photon invariant mass distribution [55]. **Middle**: limits on the SM Higgs boson production times decay branching ratio into di-photons [55]. **Right**: local probability p-values as a function of the Higgs boson mass [55]. Reproduced under the CC-BY-4.0 license.

5.2. Heavy Higgs Bosons in $pp \to A \to HZ$

In the 2HDM, $m_A > m_H$ as well as the mass ranges $m_A > 800\,\text{GeV}$, $m_H > 2m_t = 350\,\text{GeV}$ have been investigated [59]. The search final states are $tt\ell\ell$ and $bb\nu\nu$. Figure 39, upper left and right, shows the data, as well as the simulated background and signal distributions, for $tt\ell\ell$ and $bb\nu\nu$ final states, respectively, and Figure 39, lower, the resulting limits at 95% CL in the (m_A, m_H) mass parameter space [59].

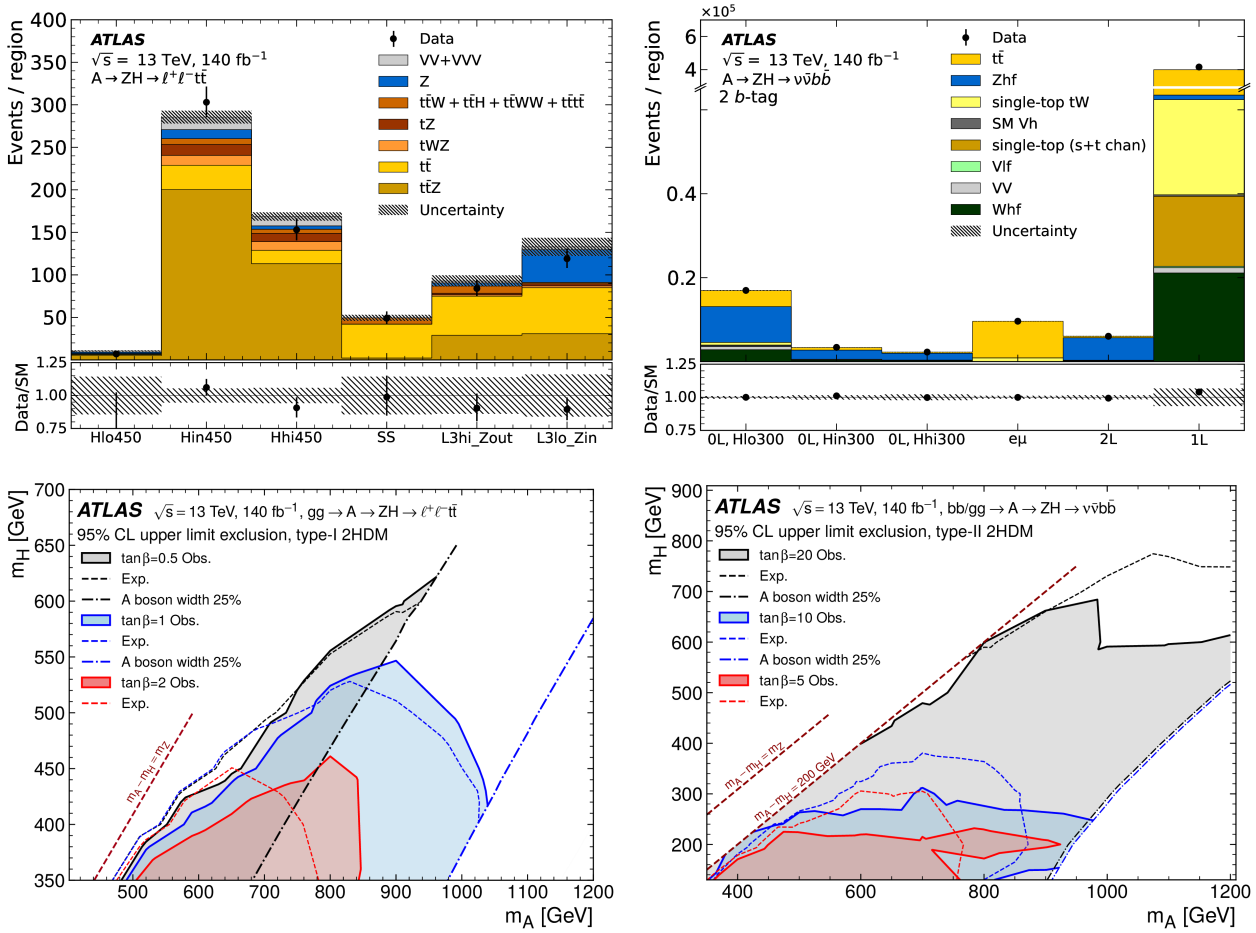

Figure 39. Upper: data, simulated background and signal distributions for $tt\ell\ell$ (**left**) and $bb\nu\nu$ (**right**) final states space [59]. **Lower**: Resulting limits at 95% CL in the (m_A, m_H) parameter space [59]. Reproduced under the copyright permission from Springer.

5.3. Heavy Higgs Bosons in $pp \to VHH$

A search for $pp \to WHH$ and $pp \to ZHH$ was performed at LHC. This resulted in limits at 95% CL on $37.7 < \kappa_\lambda < 37.2$ $(-30.1 < \kappa_\lambda < 28.9)$ and $-12.2 < \kappa_{VV} < 13.5$ $(-7.64 < \kappa_{VV} < 8.90)$ [60]. Figure 40, left, shows a Feynman diagram for the $pp \to WHH$ and $pp \to ZHH$ production, and a simulated WWH signal, and limits on the production cross-section $pp \to VHH$ are shown in Figure 40, middle and right, respectively.

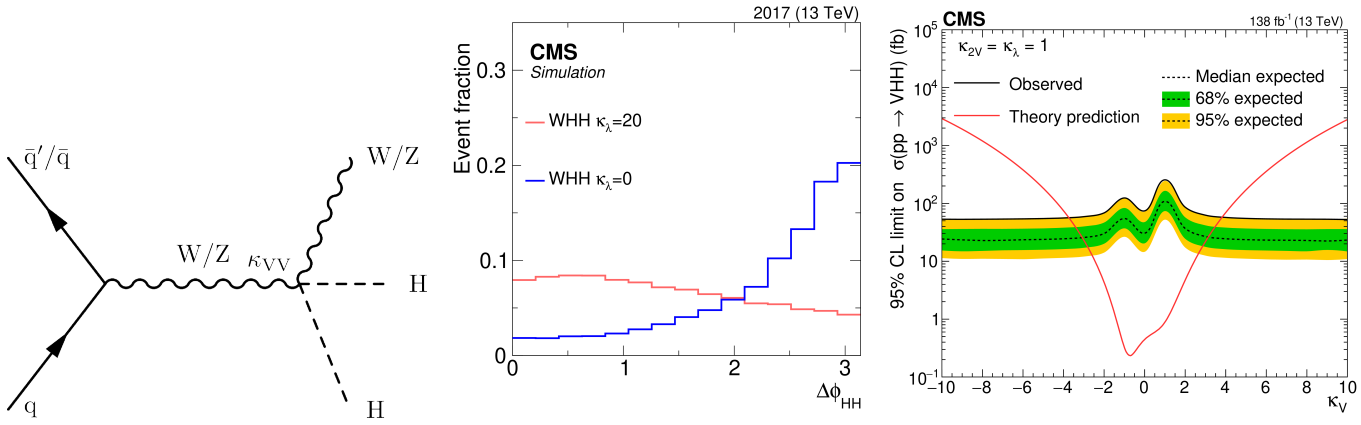

Figure 40. Left: Feynman diagram for the $pp \to WHH$ and $pp \to ZHH$ production. **Middle**: simulated WHH signal [60]. **Right**: limits on the production cross-section $pp \to VHH$ [60]. Reproduced under the CC-BY-4.0 license.

5.4. Heavy Higgs Bosons in $pp \to A \to VH, H \to hh$

A search for VH, $H \to hh$ was performed, where the vector boson decays $W \to \ell\nu$, $Z \to \ell\ell, \nu\nu$, with $\ell = e, \mu$. Interpretations have been given in the 2HDM with free parameters m_A, m_H, the ratio of the vacuum expectation values of the two Higgs doublets $\tan\beta$, and the Higgs boson coupling factor $\cos(\beta - \alpha)$ [61]. Figure 41 shows the Feynman diagram for the VH, $H \to hh$ production (Figure 41, upper left) along with the limits in the $(\cos(\beta - \alpha), m_A)$ parameter space and on the production cross-sections WH and ZH times branching ratio of $H \to hh \to bbbb$ (Figure 41, upper right, lower left and right, correspondingly) [61].

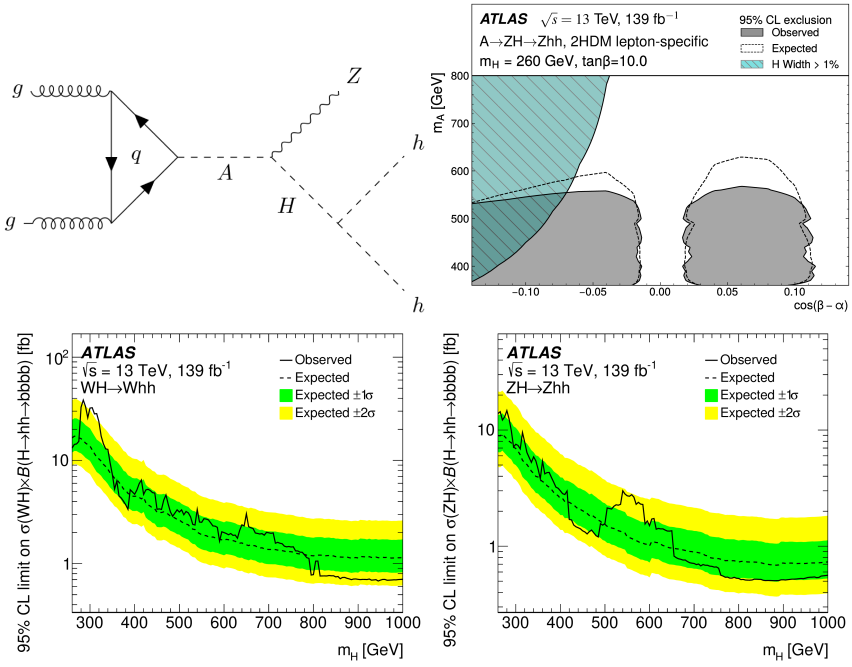

Figure 41. Feynman diagram for the VH, $H \to hh$ production (**upper left**) and the limits [61]. in the $(\cos(\beta - \alpha), m_A)$ parameter space (see text for details) (**upper right**) and on the production cross-sections WH (**lower left**) and ZH (**lower right**) times branching ratio of $H \to hh \to bbbb$. Reproduced under the copyright permission from Springer.

5.5. Heavy Higgs Bosons in $pp \to VH, H \to VV$

The search for a heavy Higgs boson in $H \to VV$ was performed in same-sign two-lepton final states (SS2l). Events with two leptons (electrons or muons) of the same electric

charge and missing transverse momentum, as well as jets, are selected. The results are interpreted in models with higher-dimensional operators in an effective field theory [62,63]. Figure 42, upper left, shows a Feynman diagram for the heavy Higgs boson production, with $H \to VV$ in same-sign two-lepton final states, while Figure 42, upper middle and right, shows the data, simulated background and $H \to VV$ signals for lepton transverse momentum and the three-lepton invariant mass distribution, respectively, along with the limits on the $pp \to VH \to H \to VV$ production cross-section and in the parameter plane (f_W, f_{WW}) in Figure 42, lower left and right, respectively, where f_W and f_{WW} are anomalous couplings to the W field.

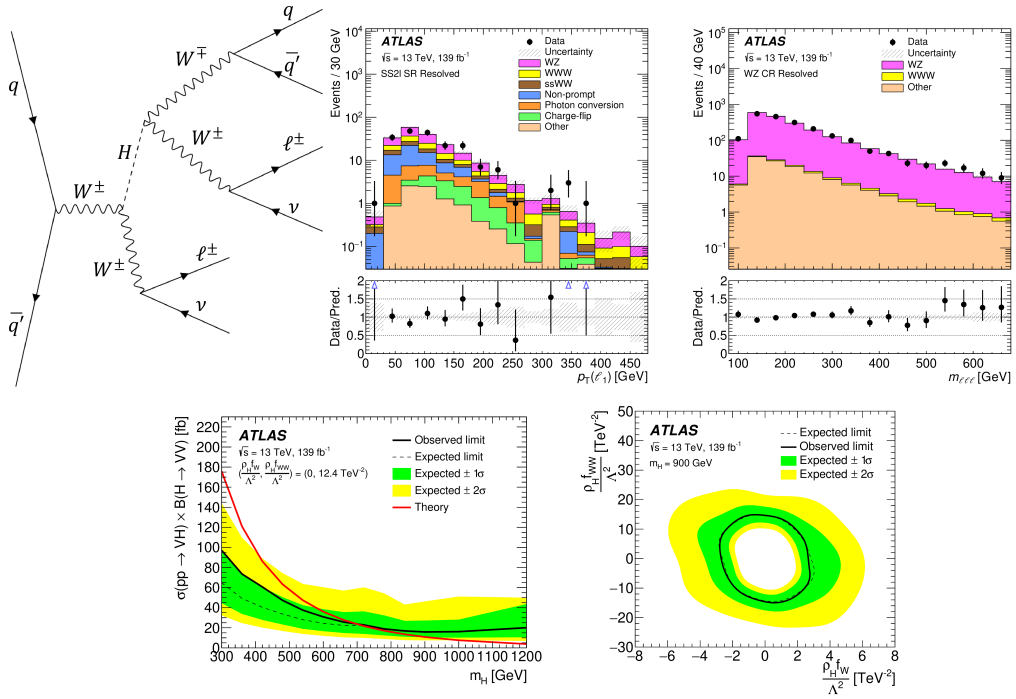

Figure 42. Upper: Feynman diagram for heavy Higgs boson production, with $H \to VV$ in same-sign two-lepton final states (**left**), data, simulated background, and $H \to VV$ signals [63] for lepton transverse momentum (**middle**) and for three-lepton invariant mass distribution (**right**). **Lower**: limits on the $pp \to VH \to H \to VV$ production cross-section (**left**) and in the parameter plane (f_W, f_{WW}) (**right**) [63]. See text for details. Reproduced under the copyright permission from Springer.

5.6. Heavy Higgs Bosons in $ttH/A \to tttt$: Multi-Lepton Final States

In the search for $ttH/A \to tttt$ multi-lepton final states, exactly two leptons with same-sign electric charges or at least three leptons are required [64]. In the 2HDM (Type-2), $\tan\beta < 1.2$ (0.5) are excluded for Higgs boson mass 400 (1000) GeV. Figure 43, upper left, shows a Feynman diagram for the $ttH/A \to tttt$ production, while the data, simulated background, and a $ttH/A \to tttt$ signal as a function of the BDT score, along with the limits on the ttH/A production cross-section times the $H/A \to tt$ branching ratio and in the $(m_A, \tan\beta)$ are shown in Figure 43, upper right, lower left and lower right, respectively.

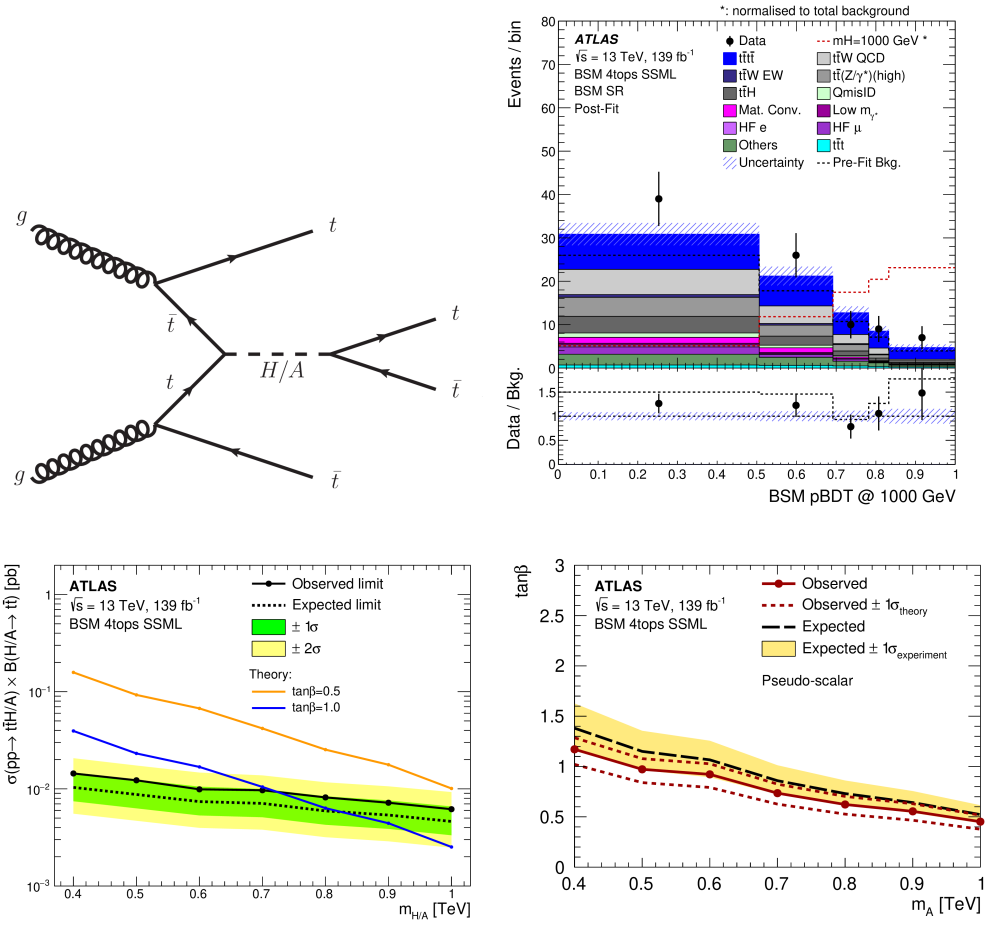

Figure 43. Feynman diagram for the $ttH/A \to tttt$ production (**upper left**); data, simulated background and a $ttH/A \to tttt$ signal (**upper right**) along with limits on the ttH/A production cross-section times the $H/A \to tt$ branching ratio (**lower left**) and exclusion limits in the $(m_A, \tan\beta)$ parameter planes (**lower right**) [64]. Reproduced under the copyright permission from Springer.

5.7. Heavy Higgs Bosons in $gg\Phi, bb\Phi, \Phi \to \tau\tau$

The search for a heavy neutral Higgs boson Φ with $\Phi \to \tau\tau$ was performed in $e\mu, e\tau_h, \mu\tau_h, \tau_h\tau_h$ final states [65]. Upper limits at 95% CL are set on the products of the branching fraction for the decay into tau leptons and the cross-sections for the production of a new boson Φ, in addition to the H(125) boson, ranging from $\mathcal{O}$ (10 pb) for a mass of 60 GeV to 0.3 fb for a mass of 3.5 TeV. Figure 44 shows Feynman diagrams for the $gg\Phi$ (Figure 44, upper left) and $bb\Phi$ (Figure 44, upper right) production, the limits on the cross-section of $gg\Phi$ and $bb\Phi$ production times branching ratio for $\Phi \to \tau\tau$ (Figure 44, lower left and right, respectively) [65], along with the limits on benchmark scenarios of the MSSM that rely on the signal from three neutral Higgs bosons, one of which is associated with H(125). Expected and observed 95% CL exclusion contours are also set in the MSSM M125 and M125(EFT) scenarios, as shown in Figure 45 [65]. The data reveal two excesses, with local p-values equivalent to about three standard deviations at 0.1 and 1.2 TeV mass.

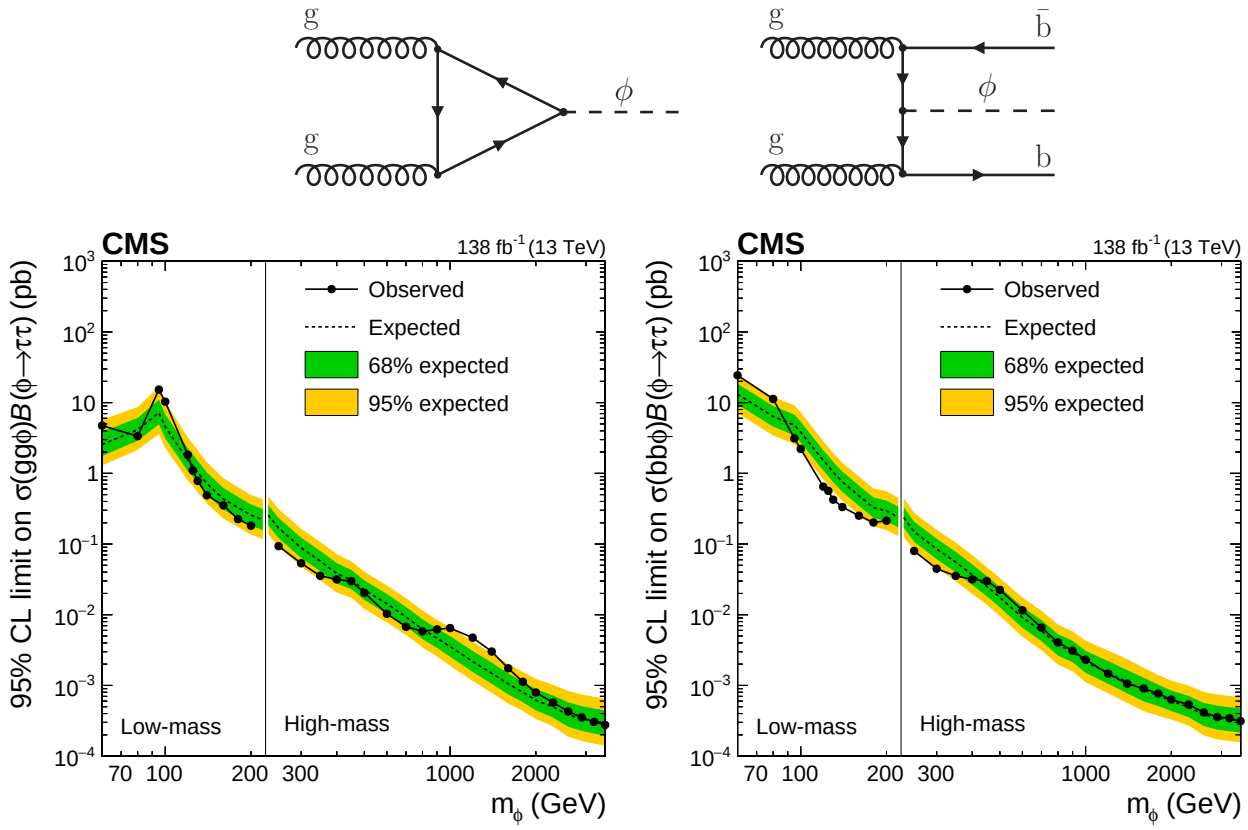

Figure 44. Upper: Feynman diagrams for the $ggΦ$ (**left**) and $bbΦ$ (**right**) production. **Lower**: limits on the cross-section for $ggΦ$ (**left**) and $bbΦ$ (**right**) production times branching ratios of $Φ \to ττ$ production [65]. Reproduced under the copyright permission from Springer.

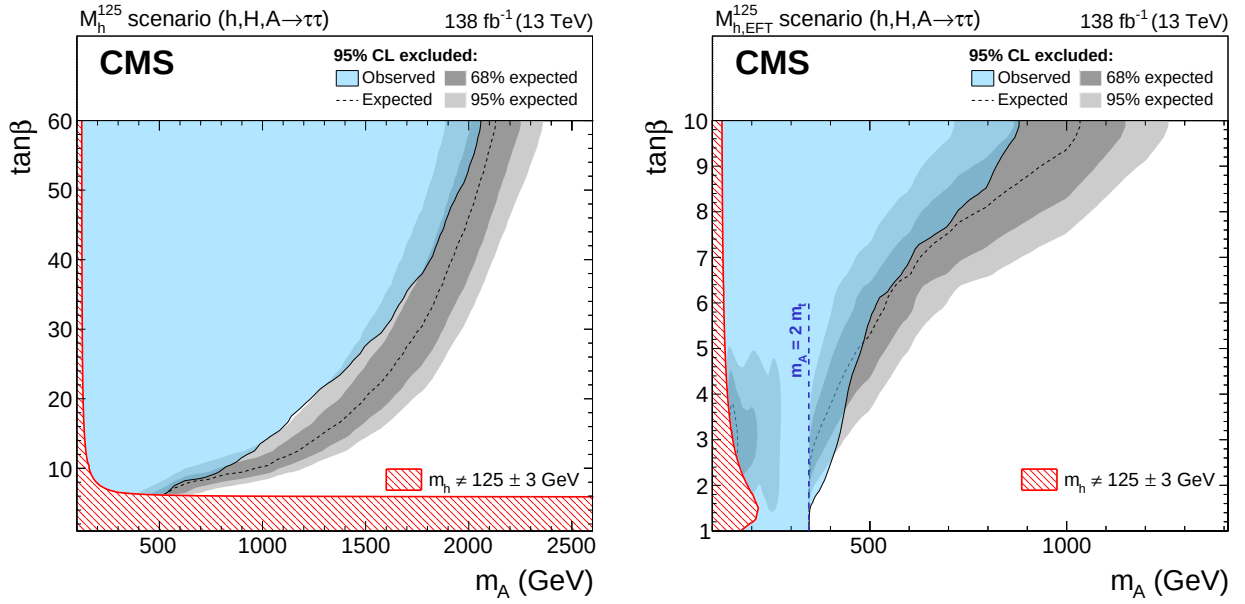

Figure 45. Expected and observed 95% CL exclusion contours for **(left)** MSSM M125 and (**right**) effective field theory M125(EFT) [65]. Reproduced under the copyright permission from Springer.

6. Higgs Bosons and Dark Matter

6.1. Dark Matter Produced in Association with a Higgs Boson Decaying into Taus

The search for DM considered to be produced in association with a Higgs boson decaying into τs was performed with the final state of two hadronically decaying tau leptons and MET, E_T^{miss}. For the interpretation, the 2HDM+a was used [66]. Figure 46, upper, shows three production Feynman diagrams leading to DM and a pair of τs and Figure 46, lower left, middle and right, shows the data, simulated background, and a DM plus τs signal, along with the exclusion limits in the (m_a, m_A) and $(m_A, \tan\beta)$ parameter planes, respectively.

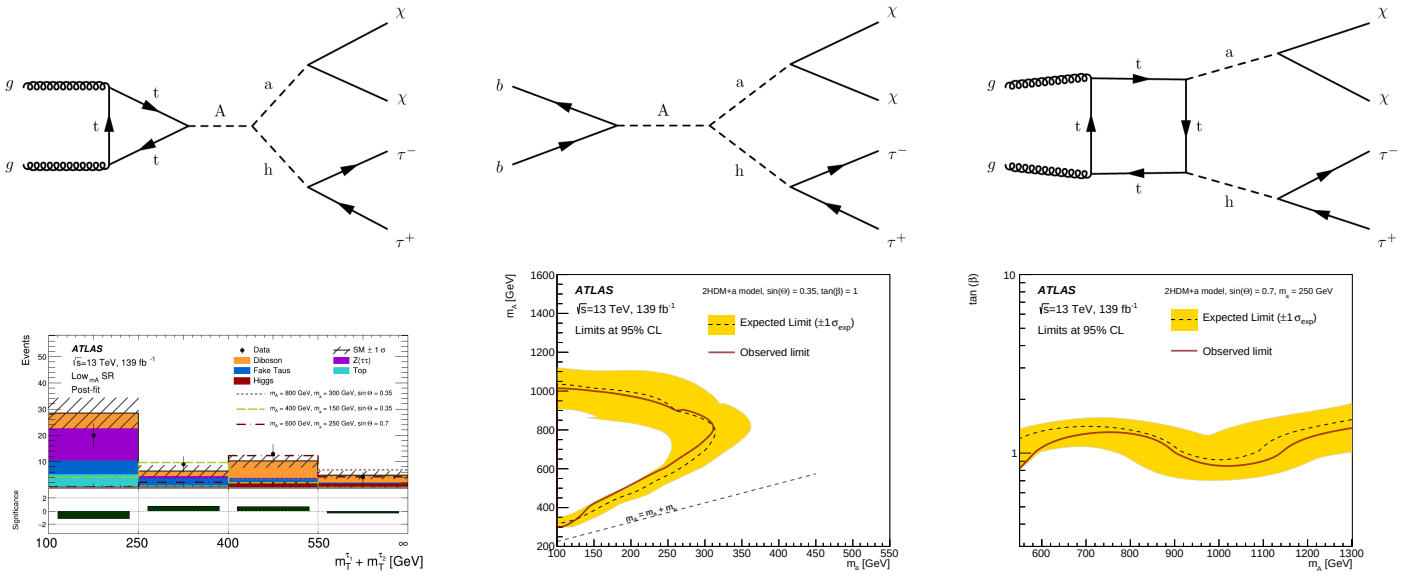

Figure 46. Upper: production Feynman diagrams leading to DM and a pair of τs. **Lower**: data, simulated background and a DM plus τs signal (**left**), exclusion limits in the (m_a, m_A) parameter plane (**middle**), and in the $(m_A, \tan\beta)$ parameter planes (**right**) [66]. Reproduced under the copyright permission from Springer.

6.2. Dark Higgs Boson

In the Dark Abelian Higgs model, an additional U(1)$_D$ gauge symmetry can lead to a dark photon, A', that mediates the dark sector interactions with the SM. The U(1)$_D$ symmetry group is spontaneously broken by a Higgs mechanism, leading to A$'$, which acquires a mass by adding a dark Higgs boson, h_D. The search for the process $Z \to A'h_D \to A'A'A^{(*)'}$ was performed, where two on-shell $A' \to \ell\ell$ with $(\ell = e\,or\,\mu)$ were required. The new results [67] were compared with results from the Belle experiment [68]. Figure 47 shows a Feynman diagram of the $Z \to A'h_D \to A'A'A^{(*)'}$ signal (Figure 47, left), data and simulated background, and $Z \to A'h_D \to A'A'A^{(*)'}$, where two on-shell $A' \to \ell\ell$, with a $(\ell = e\,or\,\mu)$ signal (Figure 47, middle) and the limits on the coupling as a function of $m_{A'}$ [67] (Figure 47, right).

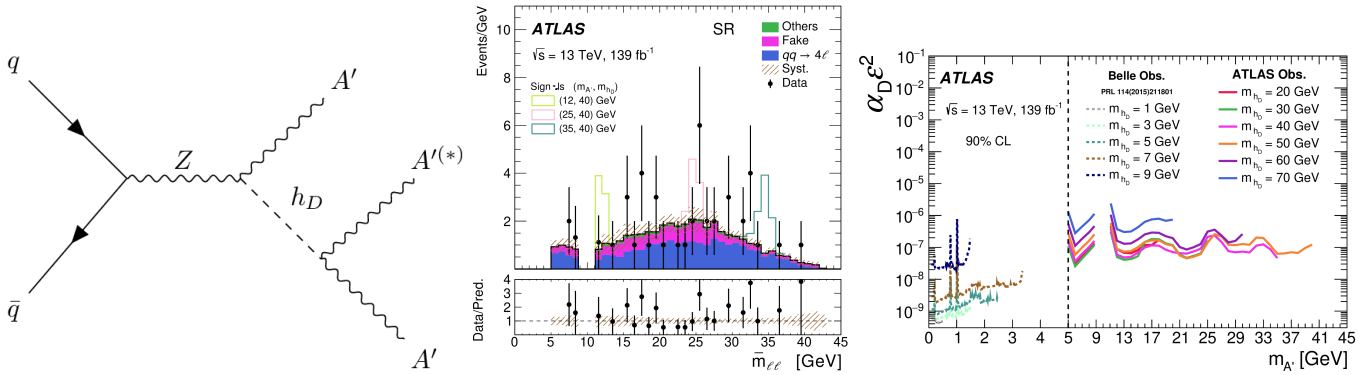

Figure 47. Left: Feynman diagram of the $Z \to A'h_D \to A'A'A^{(*)'}$ production. **Middle**: data and simulated background as well as the $Z \to A'h_D \to A'A'A^{(*)'}$ signal, where two on-shell $A' \to \ell\ell$, with a $(\ell = e/\mu e \, or \, \mu)$ signal [67]. **Right**: limits on the coupling as a function of $m_{A'}$ [67]. Reproduced under the copyright permission from the American Physical Society.

6.3. Combination of Searches in the 2HDM and Dark Matter Searches

A combination of 2HDM and DM searches was performed at LHC. The most sensitive searches were E_T^{miss} plus leptonically decaying Z bosons, E_T^{miss} plus $H \to bb$, and charged Higgs bosons with top and b-quarks decays [69]. Figure 48 shows the combined results as exclusion contours in the (m_a, m_A) parameter space.

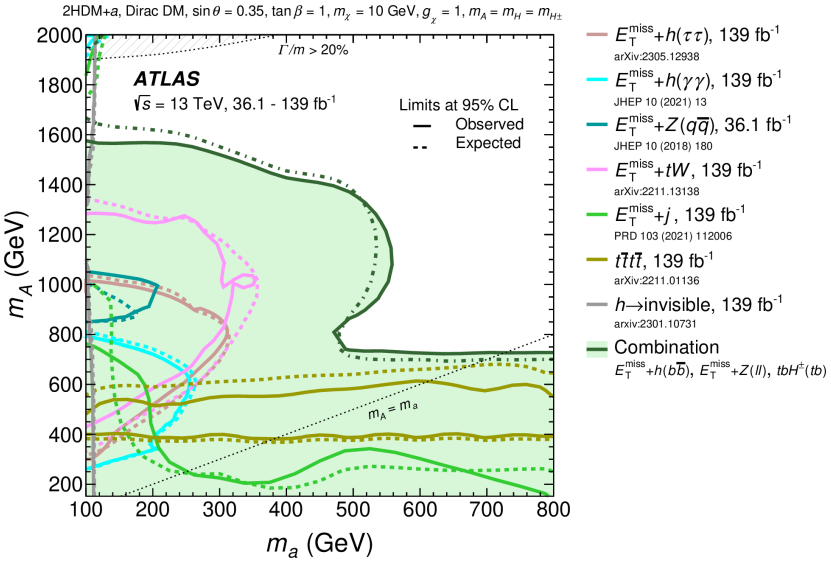

Figure 48. Results from combination of searches in the 2HDM and dark matter searches [69]. Reproduced under the copyright permission from Elsevier.

7. Additional Charged Higgs Bosons

7.1. $pp \to tt$ with $t \to H^{\pm}b$, $H^{\pm} \to W^{\pm}a$, Where $a \to \mu\mu$

The search for the process $pp \to tt$ with $t \to H^{\pm}b$, $H^{\pm} \to W^{\pm}a$, where $a \to \mu\mu$ has been performed in the mass region $15 < m_a < 72\,\text{GeV}$ and $120 < m_{H^{\pm}} < 160\,\text{GeV}$ [70]. Figure 49 shows a Feynman diagram for the charged Higgs boson production (Figure 49, left) along with the data, simulated background, and signal for the di-muon invariant mass (Figure 49, middle), and limits on the top into charged Higgs boson b-quark decay branching ratio at 95% CL (Figure 49, right). No significant excess is observed, and the smallest local p-value is 0.008 at $m_a = 27\,\text{GeV}$, corresponding to a local significance of about 2.4 s.d. The slight excess was observed at $m_a = 27\,\text{GeV}$ in both the $e\mu\mu$ and $\mu\mu\mu$ channels [70].

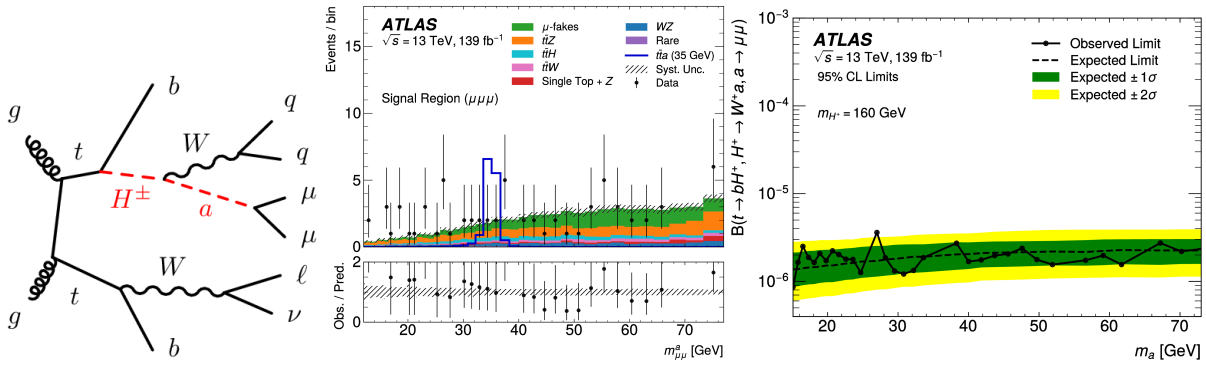

Figure 49. Left: Feynman diagram for the charged Higgs boson production. **Middle**: data, simulated background and a signal for the di-muon invariant mass [70]. **Right**: limits on the top into charged Higgs boson and b-quark decay branching ratio at 95% CL [70]. Reproduced under the copyright permission from the American Physical Society.

7.2. $t \to H^{\pm}b, H^{\pm} \to cb$

The search for $t \to H^{\pm}b, H^{\pm} \to cb$ is based on an isolated electron or muon and at least four jets and three b-tags in 3HDM [71,72]. The top quark can decay into a lighter charged Higgs boson. The couplings X, Y, and Z are the Yukawa interactions of the lighter charged Higgs boson. Those are functions of the Higgs-doublet vacuum expectation values and the mixing angle between the charged Higgs bosons [73]. Figure 50 shows a Feynman diagram of the $t \to H^{\pm}b$, $H^{\pm} \to cb$ production (Figure 50, left), data, simulated background, and a $t \to H^{\pm}b$, $H^{\pm} \to cb$ signal (Figure 50, middle), and the limits on the branching ratio $H^{\pm} \to cb$ as a function of the charged Higgs boson mass (Figure 50, right). The observed exclusion limits are consistently weaker than the expectation [73]. The largest excess in data has a local significance of about 3 s.d. for $m_{H^+} = 130\,\text{GeV}$.

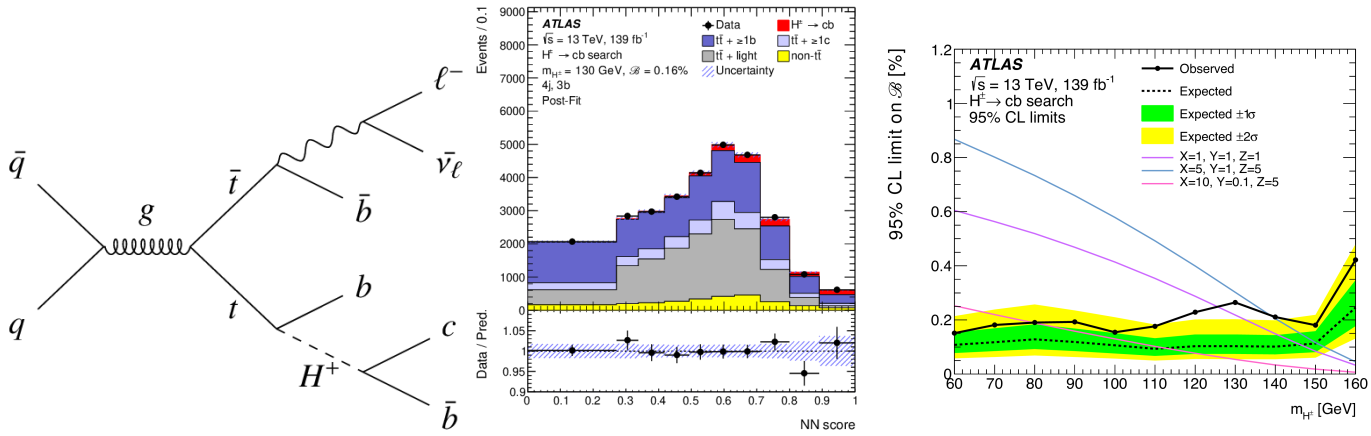

Figure 50. Left: Feynman diagram of the $t \to H^{\pm}b$, $H^{\pm} \to cb$ production. **Middle**: data, simulated background, and a $t \to H^{\pm}b$, $H^{\pm} \to cb$ signal [73] Reproduced under the CC-BY-4.0 license. **Right**: limits on the branching ratio $H^{\pm} \to cb$ as a function of the charged Higgs boson mass [73]. Reproduced under the copyright permission from Springer.

7.3. $tbH^{\pm}, H^{\pm} \to WH, H \to \tau\tau$

A search for a charged Higgs boson $tbH^{\pm}, H^{\pm} \to WH, H \to \tau\tau$ decaying into a heavy neutral Higgs boson and a W boson was performed [74]. Signal processes were generated with four mass hypotheses m_{H^+} = 300, 400, 500, and 700 GeV, under the assumption that m_h = 125 GeV and m_H = 200 GeV. Upper limits on the $tbH^{\pm}, H^{\pm} \to WH, H \to \tau\tau$ production cross-section times branching ratio were set in the range 0.085–0.019 pb for the charged Higgs bosons mass of 300–700 GeV. Figure 51, upper, shows Feynman diagrams for the process $tbH^{\pm}, H^{\pm} \to WH, H \to \tau\tau$. Figure 51, lower left and right, shows the data, simulated background along with the signal in eighteen categories (grouped into datasets represented by the vertical dashed lines) and the limits on the $tbH^{\pm}$ production cross-section times $H^{\pm} \to WH, H \to \tau\tau$ branching ratio, respectively.

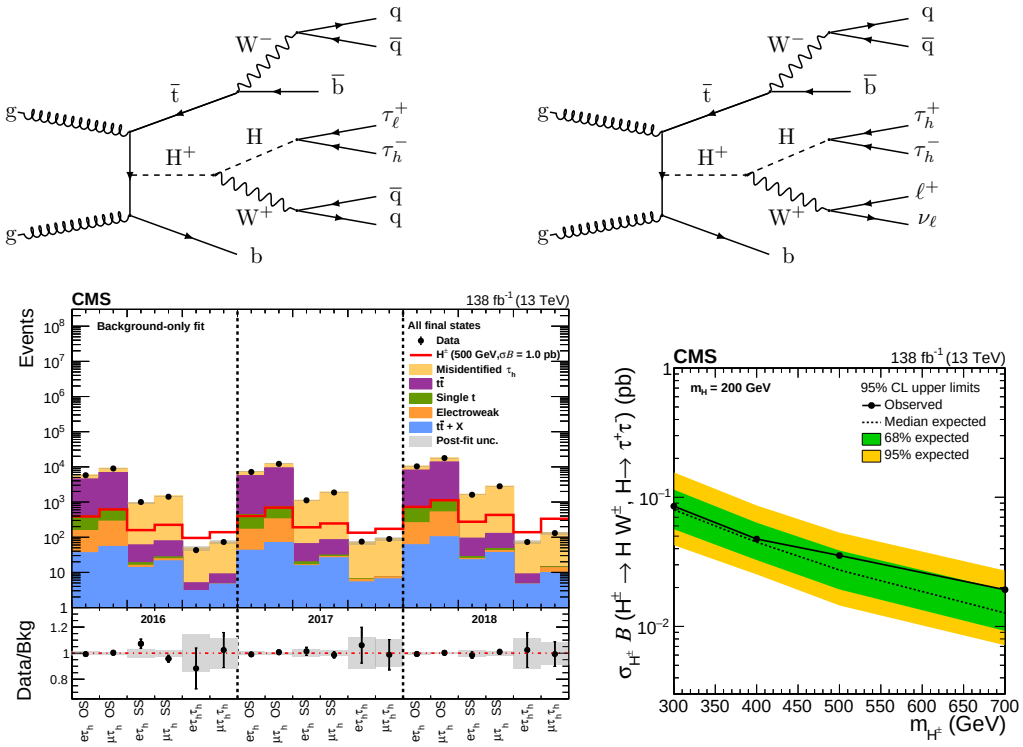

Figure 51. Upper: Feynman diagrams for the process $tbH^{\pm}, H^{\pm} \to WH, H \to \tau\tau$. **Lower left**: data, simulated background and a signal in eighteen categories grouped into datasets represented by vertical dashed lines [74]. **Lower right**: limits on $tbH^{\pm}$ production cross-section times $H^{\pm} \to WH$ and $H \to \tau\tau$ branching ratios [74]. Reproduced under the copyright permission from Springer.

7.4. Double-Charged Higgs Bosons

The search for double-charged Higgs bosons, H^{++}, has been performed in the four-lepton final state (electrons and muons). Limits on the mass of doubly charged Higgs bosons were set at 1080 GeV at 95% CL within the left–right symmetric Type-II seesaw model [75]. Figure 52, upper left, shows a Feynman diagram of the double-charged Higgs boson pair production with decay into four leptons, the data, simulated background, and H^{++} signals (Figure 52, lower), along with the limits on the production cross-section as a function of the H^{++} mass (Figure 52, upper right).

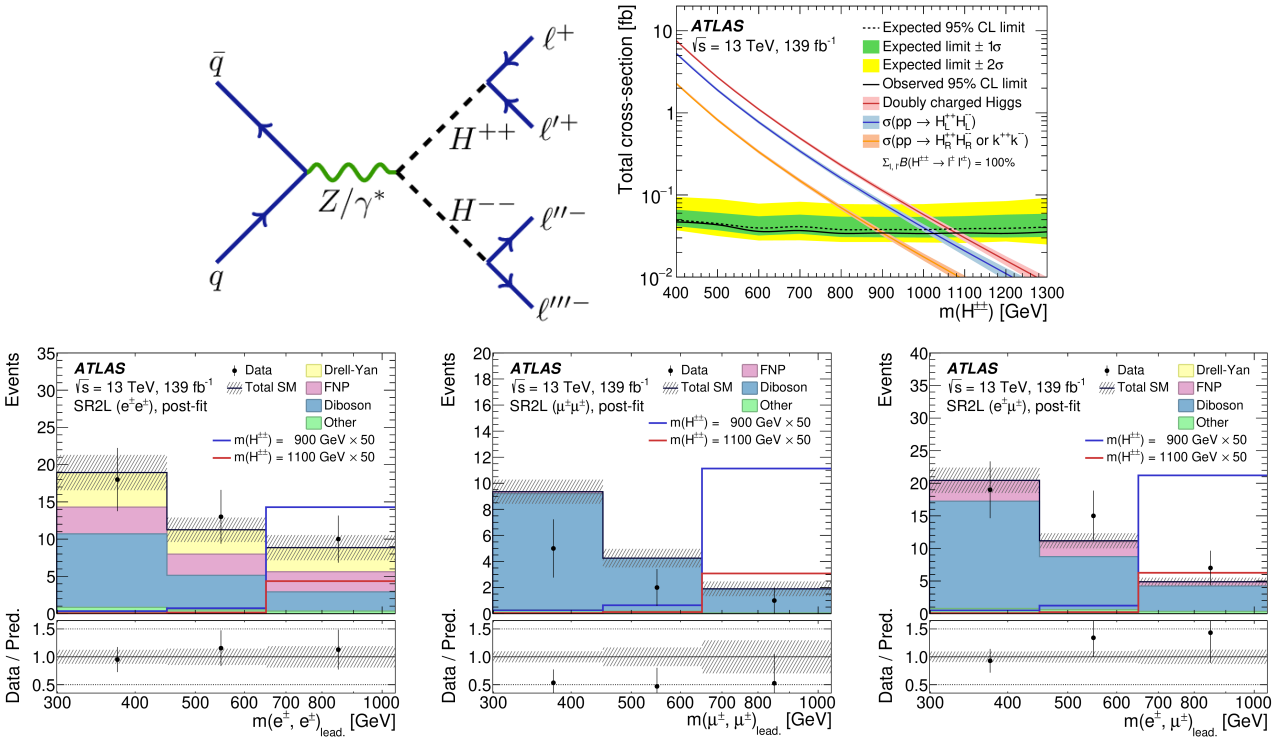

Figure 52. Upper left: Feynman diagram of the double-charged Higgs boson pair production with decay into four leptons. **Upper right**: limits on the production cross-section as a function of the H^{++} mass [75]. **Lower**: data, simulated background, and H^{++} signals [75]. Reproduced under the copyright permission from Springer.

8. Interpretations and Outlook

8.1. Interpretations of $H \to aa$ Searches in 2HDM+S

In the 2HDM+S Type-1 and Type-4, searches for $H \to aa$ with different final states [76] are summarized in Figure 53, left and middle.

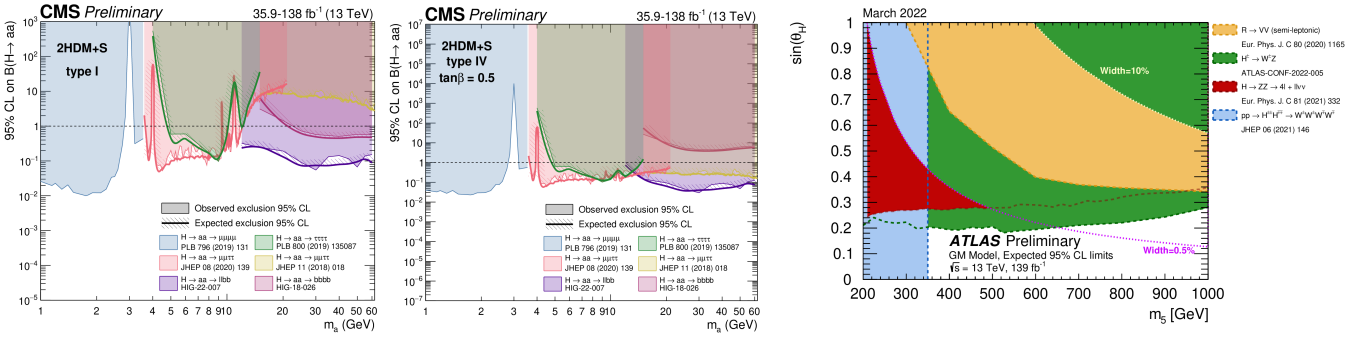

Figure 53. Left: limits on the $H \to aa$ branching ratio in the 2HDM+S Type-1 [76]. **Middle:** Limits on the $H \to aa$ branching ratio in the 2HDM+S Type-4 [76]. **Right**: limits in the $(m_5, \sin\Theta_H)$ parameter plane in the Georgi–Machacek model [77]. CMS (left, middle) and ATLAS (right) public results, reprinted under the CC-BY-4.0 license.

8.2. Interpretations of Heavy Higgs Boson Searches in the Georgi–Machacek Model

Interpretations of heavy Higgs boson searches are given in the Georgi–Machacek model [78,79]. Figure 53, right, summarizes the limits in the $(m_5, \sin\Theta_H)$ parameter plane [77], thus excluding regions of the H5 plane benchmark [8].

8.3. hMSSM Overview

Figure 54 shows an overview of the excluded regions from the ATLAS and CMS Collaborations in the MSSM with a Higgs boson at 125 GeV [80,81].

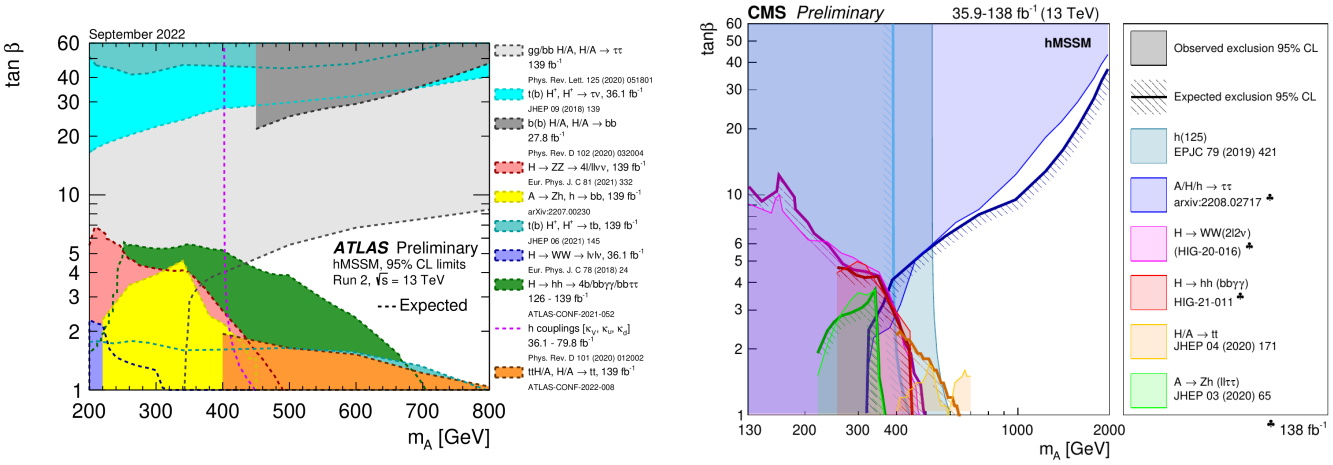

Figure 54. hMSSM summary of excluded $(m_A, \tan\beta)$ parameter regions by ATLAS [80] (**left**) and CMS [81] (**right**) Collaborations (public results). Reprinted under the CC-BY-4.0 license.

8.4. LHC Operation, Past, Present and Future

While the results presented in this Section are mostly based on the complete LHC Run-2 dataset, currently, LHC Run-3 operation is ongoing. A detailed overview of the LHC operations expectations from 2011 up to about 2040 [82] are given in Figure 55 [83].

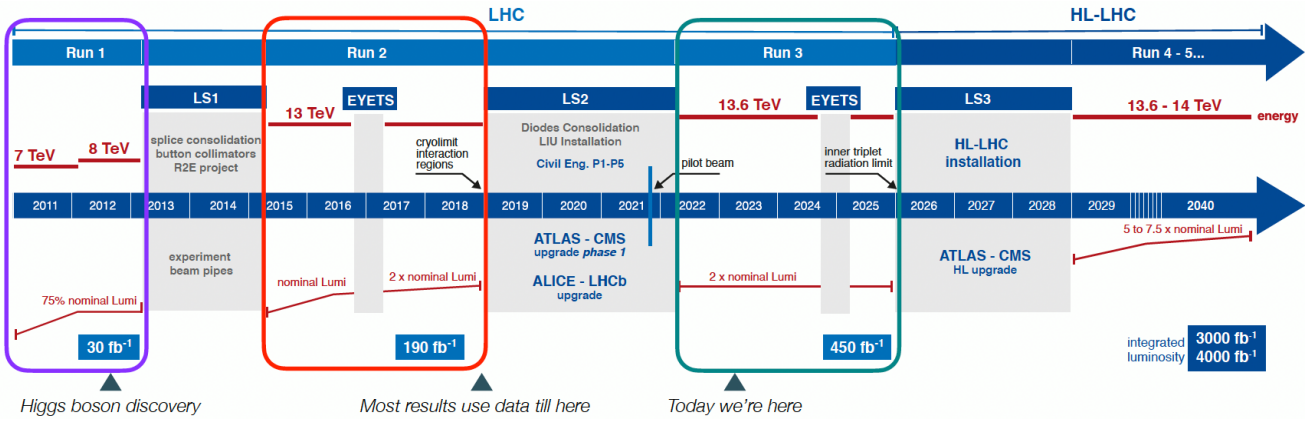

Figure 55. Overview of LHC operation in the past, present, and future [83]. Reprinted under the CC-BY-4.0 license.

9. Conclusions

The LHC operation has been highly successful. Over 160 fb^{-1} (Run-1 and Run-2 combined) luminosity was collected by each of the LHC experiments, namely, by the ATLAS and CMS experiments. Several precision measurements of Higgs boson decay branching fractions and the Higgs boson total width were performed. The relation of Higgs boson coupling to mass is impressively linear, as predicted by the Brout–Englert–Higgs mechanism. Experimental data indicate CP-invariance. In searches for rare decays, LFV, dark photons, and exotics, no indication of BSM physics was observed. In modified production modes for associated production of single top and Higgs, self-coupling HHH, and di-Higgs production, no deviation from SM expectations were observed. Limits on new Higgs bosons and unexpected decays for additional Higgs bosons decaying into taus and photons were set, as well as for heavy Higgs bosons in VHH and ttH/A production. Furthermore, limits are set to single and doubly charged Higgs boson production. As an

immediate outlook of the analysis of already recorded data, a combination of the results from the ATLAS and CMS experiments doubles statistics and thus considerably reduces the statistical uncertainties. In the current LHC Run-3 data taking period, up to 200–300 fb^{-1} luminosity data is expected to be added (years 2022 to 2025). These data will be used to draw conclusions about several observed minor excesses in Higgs boson production beyond the SM. From the year 2029, HL-LHC is aiming for 3000 fb^{-1}, starting a new era of precision measurements. There is a highly-established and well-justified LHC program until about 2040.

Funding: The project is supported by the Ministry of Education, Youth, and Sports of the Czech Republic under project number LM2023040.

Data Availability Statement: The research data are publicly shared by the ATLAS and CMS Collaboration on https://www.hepdata.net.

Acknowledgments: The author would like to thank the ATLAS and CMS Collaborations for discussions and reviews of the presented results as well as the organizers of the FFK2023 Conference for their hospitality.

Conflicts of Interest: The author declares no conflicts of interest.

Abbreviations

ATLAS	A Toroidal LHC ApparatuS
BaBar	B meson and B meson antiresonance experiment
BDT	Boosted Decision Tree
BR	Branching Ratio
BSM	Beyond SM
CC-BY-4.0	Creative Commons Attribution 4.0 International
CERN	Conseil Européen pour la Recherche Nucléaire (European Organization for Nuclear Research)
CMS	Compact Muon Solenoid
CL	Confidence Level
CP	Charge-Parity
DM	Dark Matter
EFT	Effective Field Theory
exp.	expectation(s)
FFK	Conference on Precision Physics and Fundamental Physical Constants
H	Higgs boson
HDM	Higgs-Doublet Model
HEFT	Higgs EFT
HL	High-Luminosity
H5	H_5^0
hMSSM	(LHC measured Higgs mass) m_h MSSM
ISR	Initial State Radiation
LEP	Large Electron–Positron (collider)
LHC	Large Hadron Collider
LHCb	LHC beauty
LRSM	Left–Righ Symmetric Model
LFV	Lepton Flavor Violation
MET	Missing Energy Transverse
MSSM	Minimal Supersymmetry extension of the Standard Model
M125	mass of SM Higgs boson 125 GeV
NMSSM	Next-to-MSSM
pp	proton–proton
QCD	Quantum Chromodynamics
QED	Quantum Electrodynamics
S	Singlet

SC	Signal Classification
SM	Standard Model
SS2l	Same-Sign two-lepton
s.d.	standard deviation(s)
TRSM	Two-Real-scalar-singlet extension of the SM
VBF	Vector Boson Fusion
WIMP	Weakly Interacting Massive Particle
V	Vector boson
2/3HDM	Two/Three-HDM

References

1. ATLAS Collaboration. Observation of a new particle in the search for the Standard Model Higgs boson with the ATLAS detector at the LHC. *Phys. Lett. B* **2012**, *716*, 1–29. [CrossRef]
2. CMS Collaboration. Observation of a new boson at a mass of 125 GeV with the CMS experiment at the LHC. *Phys. Lett. B* **2012**, *716*, 30–61. [CrossRef]
3. Gunion, J.; Haber, H.; Kane, G.; Dawson, S. *The Higgs Hunter's Guide*; CRC Press/Taylor & Francis Group: Boca Raton, FL, USA, 1990. [CrossRef]
4. Sopczak, A. Precision measurements in the Higgs sector at ATLAS and CMS. *PoS* **2020**, *353*, 006. [CrossRef]
5. ATLAS Experiment . Public ATLAS Luminosity Results for Run-3 of the LHC. Online Luminosity Summary Plots for Run-3. Multi-Year Summary Plots. Available online: https://twiki.cern.ch/twiki/bin/view/AtlasPublic/LuminosityPublicResultsRun3 (accessed on 30 May 2024).
6. ATLAS Experiment. Event Displays from Collision Data. 900 GeV Collisions. Available online: https://twiki.cern.ch/twiki/bin/view/AtlasPublic/EventDisplayRun2Collisions#900_GeV_Collisions (accessed on 30 May 2024).
7. CMS Collaboration. *Events Recorded by the CMS Detector During the Proton-Lead Collision Run of 2016*; Report CMS-PHO-EVENTS-2016-009; CERN: Geneva, Switzerland, 2016. Available online: https://cds.cern.ch/record/2235235 (accessed on 30 May 2023).
8. de Florian, D. et al. [LHC Higgs Working Group] *Handbook of LHC Higgs Cross Sections: 4. Deciphering the Nature of the Higgs Sector*; CERN Yellow Report CERN-2017-002-M; CERN: Geneva, Switzerland, 2017. [CrossRef]
9. ATLAS Collaboration. Luminosity determination in pp collisions at $\sqrt{s} = 13$ TeV using the ATLAS detector at the LHC. *Eur. Phys. J. C* **2023**, *83*, 982. [CrossRef]
10. CMS Collaboration. Public CMS Luminosity Information. Full Summary: Proton–Proton Collisions Since 2010 (Run 1 + Run 2 + Run 3). Available online: https://twiki.cern.ch/twiki/bin/view/CMSPublic/LumiPublicResults (accessed on 30 May 2024).
11. The ATLAS Collaboration. A detailed map of Higgs boson interactions by the ATLAS experiment ten years after the discovery. *Nature* **2022**, *607*, 52–59. [CrossRef]
12. The CMS Collaboration. A portrait of the Higgs boson by the CMS experiment ten years after the discovery. *Nature* **2022**, *607*, 60–68. [CrossRef]
13. The CMS Collaboration. Measurement of the Higgs boson width and evidence of its off-shell contributions to ZZ production. First evidence for off-shell production of the Higgs boson and measurement of its width. *Nat. Phys.* **2022**, *18*, 1329–1334. [CrossRef]
14. The ATLAS Collaboration. Evidence of off-shell Higgs boson production from ZZ leptonic decay channels and constraints on its total width with the ATLAS detector. *Phys. Lett. B* **2023**, *846*, 138223. [CrossRef]
15. ATLAS Collaboration. Measurement of the CP properties of Higgs boson interactions with τ-leptons with the ATLAS detector. *Eur. Phys. J. C* **2023**, *83*, 563. [CrossRef]
16. The CMS Collaboration. Search for CP violation in ttH and tH production in multilepton channels in proton–proton collisions at $\sqrt{s}$ = 13 TeV. *J. High Energy Phys.* **2023**, *2023*, 92. [CrossRef]
17. The ATLAS Collaboration. Test of CP-invariance of the Higgs boson in vector-boson fusion production and its decay into four leptons *J. High Energy Phys.* **2024**, *2024*, 105. [CrossRef]
18. Brivio, I.; Trott, M. The Standard Model as an effective field theory. *Phys. Rep.* **2019**, *793*, 1–98. [CrossRef]
19. The CMS Collaboration. Search for the Higgs boson decay to a pair of electrons in proton–proton collisions at $\sqrt{s} = 13$ TeV. *Phys. Lett. B* **2023**, *846*, 137783. [CrossRef]
20. The ATLAS Collaboration. A search for the $Z\gamma$ decay mode of the Higgs boson in pp collisions at $\sqrt{s} = 13$ TeV with the ATLAS detector. *Phys. Lett. B* **2020**, *809*, 135754. [CrossRef]
21. The CMS Collaboration. Search for Higgs boson decays to a Z boson and a photon in proton–proton collisions at $\sqrt{s}$ = 13 TeV. *J. High Energy Phys.* **2023**, *2023*, 233. [CrossRef]
22. Aad, G. et al. [ATLAS and CMS Collaborations]. Evidence for the Higgs boson decay to a Z boson and a photon at the LHC. *Phys. Rev. Lett.* **2024**, *132*, 0211803. [CrossRef]
23. The CMS Collaboration. Search for Higgs boson decays into Z and J/ψ and for Higgs and Z boson decays into J/ψ or Υ pairs in pp collisions at $\sqrt{s} = 13$ TeV. *Phys. Lett. B* **2023**, *842*, 137534. [CrossRef]

24. The ATLAS Collaboration. Search for exclusive Higgs and Z boson decays to $\omega\gamma$ and Higgs boson decays to $K^*\gamma$ with the ATLAS detector. *Phys. Lett. B* **2023**, *847*, 138292. [CrossRef]
25. The ATLAS Collaboration. *Summary of ATLAS Searches for Higgs and Z Boson Decays to a Meson and a Photon*; Report ATL-PHYS-PUB-2023-004; CERN: Geneva, Switzerland, 2023. Available online: https://cds.cern.ch/record/2851888 (accessed on 30 May 2024).
26. The ATLAS Collaboration. Searches for lepton-flavour-violating decays of the Higgs boson into $e\tau$ and $\mu\tau$ in $\sqrt{s} = 13$ TeV pp collisions with the ATLAS detector. *J. High Energy Phys.* **2023**, *2023*, 166. [CrossRef]
27. Hayrapetyan, A. et al. [CMS Collaboration]. Search for the lepton-flavor violating decay of the Higgs boson and additional Higgs bosons in the eμ final state in proton–proton collisions at $\sqrt{s} = 13$ TeV. *Phys. Rev. D* **2023**, *108*, 072004. [CrossRef]
28. The ATLAS Collaboration. Search for the Higgs boson decays $H \to ee$ and $H \to e\mu$ in pp collisions at $\sqrt{s} = 13$ TeV with the ATLAS detector. *Phys. Lett. B* **2020**, *801*, 135148. [CrossRef]
29. Patt, B.; Wilczek, F. Higgs-field portal into hidden sectors. *arXiv* **2006**, arXiv:hep-ph/0605188. [CrossRef]
30. The ATLAS Collaboration. Combination of searches for invisible decays of the Higgs boson using 139 fb^{-1} of proton–proton collision data at $\sqrt{s} = 13$ TeV collected with the ATLAS experiment. *Phys. Lett. B* **2023**, *842*, 137963. [CrossRef]
31. CMS Collaboration. A search for decays of the Higgs boson to invisible particles in events with a top-antitop quark pair or a vector boson in proton–proton collisions at $\sqrt{s} = 13$ TeV. *Eur. Phys. J. C* **2023**, *83*, 933. [CrossRef]
32. Clowe, D.; Bradac, M.; Gonzalez, A.H.; Markevitch, M.; Randall, S.W.; Jones, C.; Zaritsky, D. A direct empirical proof of the existence of dark matter. *Astrophys. J. Lett.* **2006**, *648*, L109–L113. [CrossRef]
33. Fabbrichesi, M.; Gabrielli, E.; Lanfranchi, G. *The Dark Photon. A Primer*; Springer Nature Switzerland AG: Cham, Switzerland, 2021. [CrossRef]
34. The ATLAS Collaboration. Search for dark photons from Higgs boson decays via ZH production with a photon plus missing transverse momentum signature from pp collisions at $\sqrt{s} = 13$ TeV with the ATLAS detector. *J. High Energy Phys.* **2023**, *2023*, 133. [CrossRef]
35. Peccei, R.D.; Quinn, H.R. Constraints imposed by CP conservation in the presence of pseudoparticles. *Phys. Rev. D* **1977**, *16*, 1791–1797. [CrossRef]
36. The CMS Collaboration. Search for an exotic decay of the Higgs boson into a Z boson and a pseudoscalar particle in proton–proton collisions at $\sqrt{s} = 13$ TeV. *Phys. Lett. B* **2023**, *852*, 138582. [CrossRef]
37. CMS Collaboration. Search for exotic decays of the Higgs boson to a pair of pseudoscalars in the $\mu\mu$bb and $\tau\tau$bb final states. *Eur. Phys. J. C* **2024**, *84*, 493. [CrossRef]
38. The CMS Collaboration. Search for direct production of GeV-scale resonances decaying to a pair of muons in proton–proton collisions at $\sqrt{s} = 13$ TeV. *J. High Energy Phys.* **2023**, *2023*, 70. [CrossRef]
39. The LHCb Collaboration. Searches for low-mass dimuon resonances. *J. High Energy Phys.* **2020**, *2020*, 156. [CrossRef]
40. Lees, J.P. et al. [BaBar Collaboration]. Search for a dark photon in e^+e^- collisions at BABAR. *Phys. Rev. Lett.* **2014**, *113*, 201801. [CrossRef] [PubMed]
41. Tumasyan, A. et al. [CMS Collaboration]. Search for exotic Higgs boson decays $H \to \mathcal{A}\mathcal{A} \to 4\gamma$ with events containing two merged diphotons in proton–proton collisions at $\sqrt{s} = 13$ TeV. *Phys. Rev. Lett.* **2023**, *131*, 101801. [CrossRef]
42. The ATLAS Collaboration. Probing the CP nature of the top–Higgs Yukawa coupling in $t\bar{t}H$ and tH events with $H \to b\bar{b}$ decays using the ATLAS detector at the LHC. *Phys. Lett. B*, **2023** *849*, 138469. . [CrossRef]
43. Sirunyan, A.M. et al. [CMS Collaboration]. Search for associated production of a Higgs boson and a single top quark in proton–proton collisions at $\sqrt{s} = 13$ TeV. *Phys. Rev. D* **2019**, *99*, 092005. [CrossRef]
44. The CMS Collaboration. Measurement of the $t\bar{t}H$ and tH production rates in the $H \to b\bar{b}$ decay channel using proton–proton collision data at $\sqrt{s} = 13$ TeV. *arXiv* **2024**, arXiv:2407.10896. [CrossRef]
45. The ATLAS Collaboration. Constraints on the Higgs boson self-coupling from single- and double-Higgs production with the ATLAS detector using pp collisions at $\sqrt{s} = 13$ TeV. *Phys. Lett. B* **2023**, *843*, 137745. [CrossRef]
46. The ATLAS Collaboration. Search for resonant and non-resonant Higgs boson pair production in the $b\bar{b}\tau^+\tau^-$ decay channel using 13 TeV pp collision data from the ATLAS detector. *J. High Energy Phys.* **2023**, *2023*, 40. [CrossRef]
47. Aad, G. et al. [ATLAS Collaboration]. Search for nonresonant pair production of Higgs bosons in the $b\bar{b}b\bar{b}$ final state in pp collisions at $\sqrt{s} = 13$ TeV with the ATLAS detector. *Phys. Rev. D* **2023**, *108*, 052003. [CrossRef]
48. The CMS Collaboration. Search for Higgs production in the b$\bar{b}$W$^+$W$^-$ decay mode in proton-proton collisions at $\sqrt{s} = 13$ TeV. *J. High Energy Phys.* **2024**, *2024*, 293. [CrossRef]
49. CMS Collaboration. Higgs PAG Summary Plots. Summary of Run-2 κ_λ and κ_{2V} measurements from HH production. Available online: https://twiki.cern.ch/twiki/bin/view/CMSPublic/SummaryResultsHIG (accessed on 30 May 2024).
50. The CMS Collaboration. Constraints on the Higgs boson self-coupling from the combination of single and double Higgs boson production in proton–proton collisions at $\sqrt{s} = 13$ TeV . *arXiv* **2024**, arXiv:2407.13554. [CrossRef]
51. The ATLAS Collaboration. Search for a new heavy scalar particle decaying into a Higgs boson and a new scalar singlet in final states with one or two light leptons and a pair of τ-leptons with the ATLAS detector. *J. High Energy Phys.* **2023**, *2023*, 9. [CrossRef]
52. The CMS Collaboration. Search for a massive scalar resonance decaying to a light scalar and a Higgs boson in the four b quarks final state with boosted topology. *Phys. Lett. B* **2023**, *842*, 137392. [CrossRef]

53. Aad, G. et al. [ATLAS Collaboration]. Combination of searches for resonant Higgs boson pair production using pp collisions at $\sqrt{s}$ = 13 TeV with the ATLAS detector. *Phys. Rev. Lett.* **2024**, *132*, 231801. [CrossRef] [PubMed]
54. CMS Collaboration. CMS Beyond SM Particles Decaying 2(to) Higgs, top and Gauge Bosons (B2G) Public Physics Results. Summary of Public Di-Boson Results (August 2023 and March 2024) . Available online: https://twiki.cern.ch/twiki/bin/view/CMSPublic/PhysicsResultsB2G (accessed on 30 May 2024).
55. The CMS Collaboration. Search for a standard model-like Higgs boson in the mass range between 70 and 110 GeV in the diphoton final state in proton–proton collisions at $\sqrt{s} = 13$ TeV. *arXiv* **2024**, arXiv:2405.18149. [CrossRef]
56. The ATLAS Collaboration. Search for diphoton resonances in the 66 to 110 GeV mass range using 140 fb^{-1} of 13 TeV pp collisions collected with the ATLAS detector. *arXiv* **2024**, arXiv:2407.07546. [CrossRef]
57. Sopczak, A. Searches for Higgs bosons beyond the Standard Model. In Proceedings of the XII International Workshop on Deep Inelastic Scattering (DIS 2004), Štrbské Pleso, Slovakia, 14–18 April 2004; Bruncko, D., Ferencei, J., Strízenec, P., Eds.; Institute of Experimental Physics SAS: Košice, Slovak Republic, 2004; pp. 1017–1022. [CrossRef]
58. Sopczak, A. A general MSSM parameter scan. *Int. J. Mod. Phys. A* **2001**, 816–818. [CrossRef]
59. The ATLAS Collaboration. Search for a CP-odd Higgs Boson decaying into a heavy CP-even Higgs boson and a Z boson in the $\ell^+\ell^- t\bar{t}$ and $\nu\bar{\nu}b\bar{b}$ final states using 140 fb^{-1} of data collected with the ATLAS detector. *J. High Energy Phys.* **2024**, *2024*, 197. [CrossRef]
60. The CMS Collaboration. Search for Higgs boson pair production with one associated vector boson in proton–proton collisions at $\sqrt{s} = 13$ TeV. *arXiv* **2024**, arXiv:2404.08462. [CrossRef]
61. ATLAS Collaboration. Search for Higgs boson pair production in association with a vector boson in pp collisions at $\sqrt{s} = 13$ TeV with the ATLAS detector. *Eur. Phys. J. C* **2023**, *83*, 519. [CrossRef]
62. Kuang, Y.-P.; Ren, H.-Y.; Xia, L.-H. Model-independent probe of anomalous heavy neutral Higgs bosons at the LHC. *Phys. Rev. D* **2014**, *90*, 115002. [CrossRef]
63. The ATLAS Collaboration. A search for heavy Higgs bosons decaying into vector bosons in same-sign two-lepton final states in pp collisions at $\sqrt{s} = 13$ TeV with the ATLAS detector. *J. High Energy Phys.* **2023**, *2023*, 200. [CrossRef]
64. The ATLAS Collaboration. Search for $t\bar{t}H/A \to t\bar{t}t\bar{t}$ production in the multilepton final state in proton–proton collisions at $\sqrt{s}$ = 13 TeV with the ATLAS detector. *J. High Energy Phys.* **2023**, *2023*, 203. [CrossRef]
65. The CMS Collaboration. Searches for additional Higgs bosons and for vector leptoquarks in $\tau\tau$ final states in proton–proton collisions at $\sqrt{s}$ = 13 TeV. *J. High Energy Phys.* **2023**, *2023*, 73. [CrossRef]
66. The ATLAS Collaboration. Search for dark matter produced in association with a Higgs boson decaying to tau leptons at $\sqrt{s} = 13$ TeV with the ATLAS detector. *J. High Energy Phys.* **2023**, *2023*, 189. [CrossRef]
67. Aad, G. et al. [ATLAS Collaboration]. Search for dark photons in rare Z boson decays with the ATLAS detector. *Phys. Rev. Lett.* **2023**, *131*, 251801. [CrossRef]
68. Jaegle, I. et al. [Belle Collboration]. Search for the dark photon and the dark Higgs boson at Belle. *Phys. Rev. Lett.* **2015**, *114*, 211801. [CrossRef]
69. The ATLAS Collaboration. Combination and summary of ATLAS dark matter searches interpreted in a 2HDM with a pseudoscalar mediator using 139 fb^{-1} of $\sqrt{s} = 13$ TeV pp collision data. *Sci. Bull.* 2024, *in press*. . [CrossRef]
70. Aad, G. et al. [ATLAS Collaboration]. Search for a new pseudoscalar decaying into a pair of muons in events with a top-quark pair at $\sqrt{s} = 13$ TeV with the ATLAS detector. *Phys. Rev. D* **2023**, *108*, 092007. [CrossRef]
71. Akeroyd, A.G.; Moretti, S.; Yagyu, K.; Yildirim, E. Light charged Higgs boson scenario in 3-Higgs doublet models. *Int. J. Mod. Phys. A* **2017**, *32*, 1750145. [CrossRef]
72. Akeroyd, A.G.; Moretti, S.; Song, M. Light charged Higgs boson with dominant decay to quarks and its search at the LHC and future colliders. *Phys. Rev. D* **2018**, *98*, 115024. [CrossRef]
73. The ATLAS Collaboration. Search for a light charged Higgs boson in $t \to H^{\pm}b$ decays, with $H^{\pm} \to cb$, in the lepton+jets final state in proton–proton collisions at $\sqrt{s} = 13$ TeV with the ATLAS detector. *J. High Energy Phys.* **2023**, *2023*, 4. [CrossRef]
74. The CMS Collaboration. Search for a charged Higgs boson decaying into a heavy neutral Higgs boson and a W boson in proton–proton collisions at $\sqrt{s} = 13$ TeV. *J. High Energy Phys.* **2023**, *2023*, 32. [CrossRef]
75. ATLAS Collaboration. Search for doubly charged Higgs boson production in multi-lepton final states using 139 fb^{-1} of proton–proton collisions at $\sqrt{s} = 13$ TeV with the ATLAS detector. *Eur. Phys. J. C* **2023**, *83*, 605. [CrossRef]
76. CMS Collaboration. Summary of 2HDM+S searches at 13 TeV (Run 2) . Available online: https://twiki.cern.ch/twiki/bin/view/CMSPublic/Summary2HDMSRun2 (accessed on 30 May 2024).
77. The ATLAS Collaboration. *Interpretation of Heavy Higgs Boson Searches in the ATLAS Experiment in the Georgi–Machacek model*. Report ATL-PHYS-PUB-2022-008; CERN: Geneva, Switzerland, 2022. Available online: https://cds.cern.ch/record/2803996 (accessed on 30 May 2024).
78. Georgi, H.; Machacek, M. Doubly charged Higgs bosons. *Nucl. Phys. B* **1985**, *262*,463–477. [CrossRef]
79. Chanowitz, M.S.; Golden, M. Higgs boson triplets with $M_W = M_Z \cos\theta_W$. *Phys. Lett. B* **1985**, *165*, 105–108. [CrossRef]
80. The ATLAS Collaboration. *Summary Plots for Beyond Standard Model Higgs Boson Benchmarks for Direct and Indirect Searches*. Report ATL-PHYS-PUB-2022-043; CERN: Geneva, Switzerland, 2022. Available online: https://cds.cern.ch/record/2827098 (accessed on 30 May 2024).

81. CMS Collaboration. Higgs PAG Summary Plots. Summary of MSSM Higgs Boson Searches at 13 TeV (Run 2). Available online: https://twiki.cern.ch/twiki/bin/view/CMSPublic/SummaryResultsHIG (accessed on 30 May 2024).
82. Longer Term LHC Schedule. Available online: https://lhc-commissioning.web.cern.ch/schedule/LHC-long-term.htm (accessed on 30 May 2024).
83. Zerlauth, M.; Brüning, O. Status and prospects of the HL-LHC project. *PoS* **2024**, *449*, 615. [CrossRef]